

**Collective Properties of
X-ray Binary Populations of Galaxies.I.
Luminosity and Orbital Period Distributions of
High-Mass X-ray Binaries**

Harshal Bhadkamkar and Pranab Ghosh

Department of Astronomy & Astrophysics, Tata Institute of Fundamental Research,
Mumbai 400 005, India

Received _____; accepted _____

ABSTRACT

We introduce a method for obtaining the X-ray luminosity function (XLF) and the binary-period distribution of populations of high-mass X-ray binaries (HMXBs) in the stellar fields (*i.e.*, outside globular clusters) of normal galaxies. We start from standard distributions of the parameters of those primordial binaries which are the progenitors of HMXBs, and follow the transformation of these distributions with the aid of a Jacobian formalism as the former evolve into the latter through the processes of the first mass transfer and the supernova (SN) that follows. We discuss the distributions of the post-SN binaries and the HMXBs. We show that our calculated model XLF has a differential slope ≈ -1.6 with a flattening at low luminosities, in excellent agreement with observations. The calculated binary-period distribution, which basically has a slightly sloping plateau-like character at intermediate periods, with a rise to this plateau at shorter periods and fall-off from it at longer periods, is in agreement with the observed distribution within observational uncertainties. We discuss the physical origin of these distributions. We demonstrate that, while the effects of both (a) the distribution of the properties of the massive companion in the HMXBs, and (b) the primordial orbital distribution and the SN dynamics are important, the former appear to be dominant in determining the XLF, and the latter in determining the HMXB binary-period distribution. We discuss the possible roles of stellar-mass black holes and ultra-luminous X-ray sources (ULX) in the observed “universal” XLF of HMXBs.

Subject headings: binaries: close – stars: neutron – stars: massive – supernovae: general – X-rays: binaries – X-rays: galaxies

1. Introduction

Four decades have passed now since the *Uhuru* discovery of the X-ray binary (henceforth XRB) Cen X-3 was first reported (Giacconi et al. 1971). What began in the early- to mid-1970s as detailed individual studies of the small number of XRBs known at the time, as also pioneering works on the construction of general models of such binaries (Lamb et al. 1973; Pringle & Rees 1972; Davidson & Ostriker 1973) has now blossomed into a mature, rich subject (for overviews, see, *e.g.*, Shapiro & Teukolsky 1983; Ghosh 2007), with a large number of XRBs discovered and catalogued today in the Milky Way, the Magellanic Clouds, and nearby external galaxies, and the fine details of the behavior of each class of XRBs well-recorded from timing and spectral studies with the aid of several generations of X-ray observatories of ever-increasing sensitivity and resolution. It is thus becoming possible now to do studies of the *collective* properties of XRB populations, obtaining statistically meaningful distributions of some of their essential properties (Kim & Fabbiano 2004; Grimm et al. 2002; Grimm et al. 2003; Gilfanov 2004; Gilfanov et al. 2004a; Gilfanov et al. 2004b; Kim & Fabbiano 2010; Liu et al. 2005; Liu et al. 2006), and exploring the essential physics underlying these distributions, which is rooted in the basic scenarios for the formation, evolution, and dynamics of XRBs (van den Heuvel 1983, 1991, 1992, 2001), which have been constructed gradually over these four decades, and which are widely accepted now. By collective properties, we mean here the distributions of X-ray luminosities and binary periods of these XRBs, the distribution of pulse periods of those binaries which exhibit periodic X-ray pulses, and perhaps also the distribution of their spectral properties at a future date.

In this series of papers, we explore the theoretical underpinnings of the observed distribution of the collective properties of XRBs in normal galaxies. We focus here on XRBs *outside* the globular clusters of these galaxies (*i.e.*, in the stellar field of the galaxy),

where the effects of encounters between XRBs and neighboring stars, as well as those between XRBs themselves, are generally thought to be negligible, due to the relatively low stellar density there. This situation is at the opposite limit to that obtaining in dense cores of globular clusters, where such encounters are thought to be *dominant* in determining the formation, evolution, and destruction of XRBs, and so their collective properties. We have studied this latter limit of XRBs in globular clusters in an earlier series of papers (Banerjee & Ghosh 2006, 2007, 2008). The current study may thus be regarded as complementary to the earlier one. We shall confine ourselves here to the distributions of X-ray luminosity and binary orbital period, since the most detailed distributions available are on these properties, and also since these properties are most readily associated with binary evolutionary characteristics. To understand the distributions of properties like pulse periods of X-ray pulsars and spectral parameters of XRBs, one must also take into account the details of the accretion torque on the neutron star, and of the X-ray emission processes. We defer these projects to the future, noting that with ~ 140 X-ray pulsars already known, the pulse-period distribution may be amenable to such a future study.

The crucial simplification that makes a straightforward approach feasible in the limit that we study here is that the absence of any significant influence on a given XRB of either the stellar background or other XRBs implies that each XRB can be thought of as evolving in *isolation*, following the well-studied and now widely-accepted scenarios for the formation and evolution of individual XRBs, starting from primordial binaries generated in normal star-formation activity in a galaxy (see, *e.g.*, van den Heuvel 2001 and the references therein). This, in turn, implies that we need only have a knowledge of the distribution of the essential parameters of these primordial binaries, and evolve these distributions through the essential processes that occur during the evolution of a primordial binary into a XRB. The task becomes even simpler when only initial and final states matter in the above processes, since we need only keep track of these states to carry out the transformation

of the relevant probability distribution, and so connect the primordial distribution to the XRB distribution in a one-to-one correspondence. This is, in fact, the case for massive or high-mass X-ray binaries (henceforth HMXBs). On the other hand, when following one or more of these evolutionary processes requires the knowledge of the entire evolution during a particular process, and not just of the initial and final states, the calculation becomes more laborious (although still straightforward in principle). This is the case for low-mass X-ray binaries (henceforth LMXBs).

In this first paper of the series, we focus our attention on HMXBs containing neutron stars. A particular circumstance that helps in this case is that, because of the short evolutionary timescales of the massive companions of the neutron stars in HMXBs, the timescale for the entire evolution from the primordial binary stage to the HMXB stage (as also the operational lifetime of the HMXB) is short (van den Heuvel 2001) compared to the timescale on which the star-formation rate (which determines the creation rate of primordial binaries) evolves (Madau et al. 1998; Ghosh & White 2001). As a consequence, the entire process we study here can be viewed as happening at a constant star-formation rate, so that the star-formation history of the galaxy adds no extra complication. Figuratively speaking, it is as if we are taking a “snapshot” of the above processes confined entirely to one epoch (the current one, $z = 0$, for the HMXB populations of the Milky Way and other local galaxies, and an appropriately earlier epoch for the HMXB populations of spiral galaxies at significant redshifts).

This argument does not, of course, apply to LMXBs, since their evolutionary timescales are comparable to or longer than (van den Heuvel 1991) those on which the star-formation rate evolves. Accordingly, we have to explicitly take into account the evolution in the star-formation rate when we apply our scheme to LMXBs, as we shall describe in later papers in the series. Thus, for example, for describing the LMXB populations of local

galaxies, we shall need to use not only the star-formation rate at $z = 0$ but also the rates at $z > 0$, *i.e.*, the star-formation history of the galaxy. This difference between the evolutionary characteristics of HMXB and LMXB populations is, of course, closely related to the earlier statement about the initial-to-final state correspondence for HMXBs versus the additional role of intermediate states for LMXBs.

In the following sections, we first describe the distributions of the essential parameters of the primordial binary populations that we adopt for our study of HMXBs, following well-established scenarios and norms in the literature. In particular, we adopt the standard initial mass function (henceforth IMF) and the standard log-uniform distribution (also known as Öpik’s law) for the orbital separation, as is done in the literature. We then describe how these parameters change in the essential processes that occur as a primordial binary evolves (van den Heuvel 2001). The first change occurs when the primary evolves, fills its Roche lobe, and transfers its envelope to the secondary, leaving behind its He core. The second change occurs when this He core finishes its further evolution, and explodes in the supernova (SN) that creates the neutron star. We give explicit relations connecting the binary parameters in the initial and final states of these two processes. Using these relations, we show how the standard rules of probability transformation enable us to derive the distributions of the post-SN binary parameters from the original primordial binary parameters through the Jacobian formalism. Next, we consider what happens when the massive companion to the neutron star evolves off the main sequence, becoming a giant/supergiant, and driving a strong stellar wind, from which the neutron star accretes matter, thus turning on the HMXB phase (van den Heuvel 2001).

We adopt standard stellar-wind models from the literature and show how we can derive the distributions of both the X-ray luminosities L_X and the orbital periods P_{orb} of the HMXBs from the distributions we obtained above. We then compare our calculated distributions with

the observed distributions of L_X (Grimm et al. 2002; Gilfanov 2004; Gilfanov et al. 2004a) and P_{orb} (Liu et al. 2005; Liu et al. 2006) reported in the literature. We show that the main feature of the observed L_X -distribution, *viz.*, the power-law behavior with a differential slope $dN/dL_X \approx -1.6$ over a wide range of L_X (Gilfanov 2004) is reproduced well in our calculated distribution over the luminosity range covered by neutron-star HMXBs. At the lowest luminosities, below the range covered in the above observational work, our calculated distribution shows a shallower rise in dN/dL_X with decreasing L_X . We show that this feature is consistent with recent observations (Shtykovskiy & Gilfanov 2005a,b) of the Magellanic Clouds. For the P_{orb} -distribution, we show that the general features of the observed distribution are in reasonable agreement with the results of our calculations within observational uncertainties.

Subsequent sections of the paper are arranged as follows. In Sec.2, we give a brief overview of the formation of neutron-star HMXBs from primordial binaries and their subsequent evolution, and we describe the standard distribution of primordial binary parameters that we adopt. In Sec.3, we describe how the binary parameters evolve through the processes of (a) the first mass transfer in the system and (b) the subsequent supernova of the He-core of the primary. In Sec.4.1, we introduce the Jacobian formalism for calculating how the distribution of binary parameters transforms as these parameters evolve as described in the previous section. In Sec.4, we discuss the distribution of the essential parameters of the post-SN binary. In Sec.5, we detail the evolution of the post-SN binary into a HMXB, summarizing the essentials of the stellar and stellar-wind models that provide these details, and indicating the further transformation of distributions needed at this point. In Sec.6, we discuss our calculated HMXB distributions of luminosity (*i.e.*, the X-ray luminosity function or XLF) and binary period, compare them with observed distributions, and discuss the effect on our model calculations of varying essential inputs like the initial mass function (IMF), stellar wind models, and so on. Finally, in Sec.7, we

discuss our results from various angles, including issues about primordial binary parameters, roles of Be-star binaries and black holes, physical origins of some essential features of the HMXB distributions, and then summarize our conclusions and future outlook. Details of some of our calculational methods are summarized in Appendix A.

2. HMXB Formation and Evolution

Scenarios for the formation and evolution of HMXBs have been studied in detail since the early 1970s, and a “standard” picture has now emerged, which is very well-documented (van den Heuvel 1983; van den Heuvel 1991; van den Heuvel 1992; van den Heuvel 2001), thus making it unnecessary to recount it here in detail. Very briefly, one starts with a primordial binary of two massive stars. The more massive of the two (*i.e.*, the primary) evolves faster, ends its main sequence life and expands rapidly to become a giant, the whole process occurring on a timescale of $\sim 10^6 - 10^7$ years. The giant overflows its Roche lobe and starts transferring its hydrogen envelope to the secondary, at which point there are two possibilities, depending on the ratio of the thermal timescales of the two stars, which, in turn, depends on their mass ratio. The first possibility arises if the mass ratio is not so extreme (quantitative arguments are given in the next section) that the above two timescales are not different by more than an order of magnitude, say. The secondary can then accept the entire mass transferred by the primary. This leaves behind only the He-core of the primary, and the secondary becomes so massive after assimilating the H-envelope of the primary that it in fact turns into the more massive component of the system. This is the channel through which HMXBs form. The second possibility arises if the mass ratio is so extreme that the thermal timescales are disparate by more than the above amount, in which case the secondary is unable to accept the mass transferred by the primary, and this mass forms a common envelope (CE) surrounding the secondary and the He-core of the

primary. This is the standard channel through which LMXBs are thought to form, which we do not discuss further in this paper.

In the HMXB channel, the system now consists of a He-core plus a massive star, which was the secondary earlier, but is now the more massive component. The He-core finishes the rest of its evolution rapidly (in $\sim 10^5 - 10^6$ years), and explodes in a supernova, leaving behind a neutron star which will become the main X-ray emitter in the HMXB. The massive companion to the neutron star now finishes its main-sequence evolution in $\sim 10^6$ years, expands to become a supergiant, and drives a strong stellar wind. Accretion from this wind by the neutron star generates X-rays, and the system thus turns on as a HMXB. This HMXB phase lasts $\sim 10^4 - 10^5$ years, after which the massive companion fills its Roche lobe. The subsequent mass-transfer is very large and rapid, which leads to considerable mass loss from the system, formation of a common envelope (CE) surrounding the neutron star and the He-core of the evolved massive companion, and a total extinction of the X-ray source. The outcome of this CE evolution, *viz.*, the formation of a compact binary consisting of the neutron star and the He-core of its former massive companion, which, after the SN of this He-star, ultimately leads to the formation of a double-degenerate system consisting either of an eccentric double-neutron-star binary or of two runaway single neutron stars (van den Heuvel 2001), lies outside the scope of this work.

In recent years, variations, modifications and additions to the above standard scenario have been considered. For example, it has been suggested that CE evolution of sufficiently wide systems during the first mass transfer may still lead to tight post-CE systems which would contribute to HMXB production (see (Linden et al. 2009) and references therein), and that these systems might remain tight even after the SN explosion, turning promptly into HMXBs with unevolved companions. Further, under certain other circumstances, CE evolution might lead to tightly-bound HMXBs with He-rich donors (Linden et al. 2009).

In this first look at the problem, we shall not consider these fascinating possibilities, but rather confine ourselves to the standard picture, since our aim here is to assess the viability of our approach in the simplest testing ground, before attempting further refinements.

2.1. Primordial Binary Distribution

We consider now the distribution of the essential properties of the primordial binaries from which HMXBs evolve according to the standard scenario sketched above. The progenitor primordial binary system is described by three essential properties, namely, the mass of primary (M_p), the mass of the secondary (M_s), and the orbital separation (a_0). An equivalent description is in terms of M_p , the mass ratio $q = M_s/M_p$, and a_0 . We use the second description throughout this work, following the custom of recent literature on the subject, and briefly mention the correspondence between the two descriptions in Sec.7.1. Also, as is often done in this subject, we take the primordial binary orbits to be circular for the purposes of the problem we study here.

The constraints imposed by the HMXB problem under consideration here limits the allowed range of the above parameters. If we restrict ourselves to only neutron-star HMXBs, as we do in this paper, then the primary mass M_p is restricted to be between roughly $9M_\odot$ and $30M_\odot$ (Heger et al. 2003). This means, of course, that those HMXBs which have black holes (either stellar-mass or intermediate-mass) as their compact, X-ray emitting components are outside the scope of this work. We return to this point in Sec.7.3. Next, the secondary mass M_s is restricted from below by the requirement mentioned above, *i.e.*, that its thermal timescale must not be larger than that of the primary by more than one order of magnitude, which implies a rough lower bound $M_s \geq 0.3M_p$, since the thermal timescale goes roughly as the inverse square of the mass in this mass-range. The upper bound on M_s is of course $M_s \leq M_p$ by definition. This means, therefore, that the allowed range of

the primordial-binary mass ratio is roughly $0.3 \leq q \leq 1$ for HMXB formation. Finally, the initial orbital separation a_0 is restricted from above by the condition of Roche lobe overflow when the primary evolves off the main sequence, without which there would be no mass transfer, and the stipulated HMXB formation scenario will not operate. It is customary to take this upper limit as $a_0 \leq 10^3 R_\odot$, which is not very restrictive.

Consider now the distributions of M_p , q , and a_0 we use in this work, in keeping with the common practice in the literature. The M_p -distribution is described in terms of a suitable Initial Mass Function (IMF), *i.e.*, the probability density $f_M(M)$ of a stellar mass being in the range M to $M + dM$. The IMF is widely taken to be of a power-law form $f_M(M) \propto M^{-\alpha}$, the classic Salpeter IMF (Salpeter 1955) corresponding to $\alpha = 2.35$, and a more recent suggestion being $\alpha = 2.7$ (Kroupa & Weidner 2003). We adopt the Salpeter IMF for our main calculations and study the effect of varying the IMF on the L_X -distribution in Sec.6.4.2.

The q -distribution is generally taken as a power-law in q , given by $f(q) \propto q^\beta$, where the exponent β may depend on the type of XRB population being studied. Following the usage in recent works on population studies of HMXBs (Belczynski et al. 2008; Linden et al. 2009), we adopt a uniform q -distribution, $\beta = 0$, in our HMXB studies in this paper. (However, we do note that our formalism has the provision for handling non-uniform distributions of q , which will indeed be used in our LMXB studies described in subsequent papers in this series.)

The distribution of the orbital separation a_0 is almost universally taken in the literature to be a loguniform one (*i.e.*, an equal number of systems in equal intervals of $\log a_0$), also known as Öpik’s law (Öpik 1924). This implies a probability density $f(a_0)$ of the separation being in the range a_0 to $a_0 + da_0$ as $f(a_0) \propto 1/a_0$. We adopt Öpik’s law in our work.

In order to construct the total probability distribution function of primordial binaries,

we need only note that the above pieces of the probability density function (PDF) are independent of each other, subject to the restrictions in the allowed ranges of values detailed above. Thus, subject to these restrictions, the total PDF is given by:

$$f_{\text{primo}}(M_p, q, a_0) = \frac{1}{N} \frac{M_p^{-\alpha}}{a_0} \quad (1)$$

Here N is a normalization parameter. Note that, although this PDF is mathematically defined over much larger ranges of parameters, we are interested only in the allowed range for HMXB formation, as explained above. Hence, we set $f_{\text{primo}} = 0$ over the forbidden range, and so choose the normalization parameter N that the integral of the PDF over the allowed range is unity. Consequently, although this PDF has no explicit dependence on q due to the assumed uniform q -distribution for this HMXB study, the allowed range of q , *i.e.*, $0.3 - 1$, does have an effect on the value of N .

3. Evolutionary Changes in Binary Parameters

In this section, we summarize the changes in the binary parameters as the system evolves through the first mass-transfer phase, and the subsequent SN of the He-core of the original primary. As mentioned in Sec.1, these changes only require keeping track of the relations between the initial and final states in each of the above two processes, which makes the ensuing transformations relatively simple.

3.1. First mass transfer

In keeping with previous work on the subject, we assume that there is negligible mass loss from the system during this process, *i.e.*, the mass transfer is *conservative*, so that the H-envelope of the primary is entirely transferred to the secondary, leaving behind its

He-core of mass $M_{p,c}$ given by:

$$M_{p,c} = M_0 M_p^{1/\xi}, \quad (2)$$

where typical values of M_0 and ξ used in the literature are $0.073M_\odot$ and 0.704 respectively, for a metallicity of $z \approx 0.03$. This is a commonly-used analytic approximation to the results of numerical stellar-evolution calculations (Ghosh 2007 and references therein).

Because the mass transfer is conservative, the binary parameters \bar{M}_p , \bar{M}_s , and \bar{a} at the end of it are related to the primordial binary parameters as:

$$\begin{aligned} \bar{M}_p &= M_{p,c} , \\ \bar{M}_s &= M_p + M_s - M_{p,c} , \end{aligned} \quad (3)$$

and

$$\bar{a} = a_0 \left[\frac{M_p M_s}{\bar{M}_p \bar{M}_s} \right]^2 . \quad (4)$$

3.2. Supernova

The post-mass-transfer binary is detached. The He-core described above evolves further and explodes as a supernova (SN), which leaves behind a neutron star of a typical mass of $1.4 M_\odot$ and blows off the rest of the He-star. This sudden mass loss from the system alters the orbital separation and makes the orbit eccentric. We assume in this work that the neutron star has the above mass in all cases. Neglecting any effects of the expanding supernova ejecta on the secondary, *e.g.*, ablation, the secondary remains completely unchanged in this process. Since we assume that the mass of the neutron star is always fixed to $1.4 M_\odot$, it can no longer be used formally as a free parameter in the description of the post-SN system. Therefore, we choose the orbital eccentricity e as the third parameter, so that the post-SN system is described by the companion mass (M_c), the semimajor axis (a) and the eccentricity (e).

Natal supernova kicks introduce additional changes in the post-SN parameters. It is generally believed today that the SN explosion need not have exact spherical symmetry. Many suggestions have been given for the physical origin of this asymmetry, *e.g.*, density inhomogeneity in the pre-collapse core, anisotropic neutrino emission, unequal momentum fluxes in the jet and anti-jet directions, and so on (Scheck et al. 2004; Scheck et al. 2006). It has also been pointed out that a seed anisotropy, once introduced by these mechanisms, will be enhanced during the hydrodynamic evolution of the explosion and may impart a large kick to the neutron star. Proper motion measurement of radio pulsars is used as a diagnostic of these natal kicks. Such studies have shown that the distribution of the pulsar velocities can be described by a 3D isotropic Maxwellian, in which the kick speed v is distributed as $f(v) \propto v^2 \exp(-v^2/2\sigma^2)$ (Hobbs et al. 2003), with $\sigma = 265$ km/s (Hobbs et al. 2003), and the direction of the kick velocity is distributed isotropically. Earlier works had suggested that the distribution might actually be bimodal, represented by two Maxwellians, so that the overall distribution would be the weighted sum of these (Arzoumanian et al. 2002).

Recent works have argued that electron-capture supernovae (ECSN) are likely to produce much lower kicks with $\sigma \approx 50$ km/s or lower (Linden et al. 2009), while the larger value given in the previous paragraph is appropriate for iron-core-collapse supernovae (ICCSN). We note here that studies of the proper motions of pulsars involve single pulsars, some of which would have come from a single star collapse. For the rest, which were obtained by disruption of binary systems, there would clearly be an observational bias towards higher kick velocities, since it is these systems which became preferentially unbound to yield the single pulsars whose proper motions are studied observationally. However, such effects are difficult to account for at this stage of understanding of the problem, and it is customary in the literature to apply the inferred distribution of kick velocities directly to the X-ray binary progenitors, as we have done here.

Effects of isotropic Maxwellian SN-kicks in progenitors of X-ray binaries were studied in a pioneering work by Kalogera (1996). For our study here, we have devised a method related to that described in the above work, but designed specifically for our purposes here. The method works as follows. If we define our co-ordinate system such that, just before the SN explosion, the line joining the two stars is along the x-axis and the neutron star is moving in the positive z-direction with a keplerian orbital velocity v_{orb} , then a kick of magnitude v_k in the direction $\hat{n}(\theta, \phi)$ would produce a change in orbital parameters given by:

$$\begin{aligned} \frac{M_i^t}{a_i} + v_k^2 + 2v_k \cos\theta \sqrt{\frac{M_i^t}{a_i}} &= M_f^t \left(\frac{2}{a_i} - \frac{1}{a_f} \right) \\ a_i^2 \left[v_k^2 \sin^2\theta \sin^2\phi + \left(\sqrt{\frac{M_i^t}{a_i}} + v_k \cos\theta \right)^2 \right] &= M_f^t a_f (1 - e^2) \end{aligned} \quad (5)$$

Here the angles θ and ϕ are defined in the usual way, M^t denotes the total mass of the system, and the subscripts i and f denote the initial and final values (*i.e.*, *pre-SN* and *post-SN* values). All quantities here are in solar units, with v in the units of $\sqrt{GM_\odot/R_\odot}$.

Due to the Maxwell-distributed random SN-kicks given to the neutron star, the one-to-one correspondence between the pre-SN and post-SN binary parameters, which would have existed in the absence of such kicks, is broken now. Instead, we need to calculate a suitable *average* effect of SN-kicks on the transformation between the pre-SN and post-SN parameters, which takes into account the underlying distribution of the kicks. To this end, we average eqs.5 over the distribution of v_k , upon which the linear terms in $v_k \cos\theta$ vanish due to isotropy, and the distribution-averaged transformation equations become:

$$\frac{M_i^t}{a_i} + v_k^2 = M_f^t \left(\frac{2}{a_i} - \frac{1}{a_f} \right)$$

$$a_i^2 \left(\frac{M_i^t}{a_i} + \frac{2}{3} v_k^2 \right) = M_f^t a_f (1 - e^2) \quad (6)$$

Here, v_k^2 is v^2 averaged over the kick-distribution. For a Maxwellian distribution, it is given by:

$$\langle v^2 \rangle = \frac{\int v^4 \exp(-v^2/2\sigma^2) dv}{\int v^2 \exp(-v^2/2\sigma^2) dv} \quad (7)$$

Those properties of v_k^2 for a Maxwellian which we need for our work are detailed in Appendix A. We assume here a combination of two Maxwellians with values of σ appropriate for ICCSN and ECSN, as described above. The way for determining the appropriate proportions of these two components is described below in Sec.4.2. For each of the two components, the parameter transformations are also given in Appendix A.

4. Post-SN probability density function

4.1. Jacobian formalism

Probability theory provides us with a method of transforming the PDF of a set of variable to the PDF of another set of variables, if we know the relations between the these two sets of variables. Let us assume that a system is described by a set of variables denoted by a vector \bar{X} . A given specific process transforms this set of parameters to another set of (the same number of) parameters denoted by \bar{Y} . Both the forward transformation $\bar{Y}(\bar{X})$ and the inverse transformation $\bar{X}(\bar{Y})$ are mathematically defined. The initial PDF as a function of \bar{X} , $f_X(\bar{X})$ then transforms as follows:

$$f_Y(\bar{Y}) = f_X(\bar{X}(\bar{Y})) \left| \frac{\partial \bar{X}}{\partial \bar{Y}} \right| \quad (8)$$

Here, $\left| \frac{\partial \bar{X}}{\partial Y} \right|$ is called the Jacobian determinant of the inverse transformation. The above theorem can now be applied to our problem in order to transform the PDF of the primordial binaries to the post-SN PDF.

4.2. Inverse transformation and post-SN PDF

In order to apply the above formalism to our problem, we need to invert the above parameter transformation relations, which is straightforward. The Jacobian of this transformation (J_{mtr}) can also be readily calculated. In the two regions described in Appendix A, these transformations can be obtained and the Jacobian (J_{sn}) can be calculated explicitly, as detailed in Appendix A.

Working in either region, the post-SN PDF is given by:

$$\bar{f}_{psn}(M_c, e, a) = f_{primo} J_{mtr} J_{sn} \quad (9)$$

The PDF of the parameters of the post-SN binary, M_c, e, a , no longer factorizes into individual PDFs for these three parameters, unlike the situation for the PDF of primordial binaries. This is as expected, since the parameter transformation laws given above mix the parameters. An immediate consequence of this is that the PDF for any one of the above post-SN binary parameters needs to be obtained by integrating the PDF of Eqn.9 over the other two parameters.

As described above, we use two values of the dispersion in the kick distribution, σ , appropriate for ICCSN and ECSN. We have also described above the method of calculating the distribution in each case. The actual distribution of the parameters with both types of SN present is the weighted sum of these two PDFs for the two values of σ , and this weighting comes from the following considerations. For the range of M_p which leads to ECSN events,

we have adopted here the value advocated in recent works (Podsiadlowski et al. 2004), which is $8-11 M_{\odot}$. The relative contribution of the ECSN and ICCSN is then given by $N_{EC}/N_{ICC} = N(M_{min}, M_{tran})/N(M_{tran}, M_{max})$, which depends upon the IMF. Here, $M_{min} = 9M_{\odot}$, $M_{max} = 30M_{\odot}$ define the allowed range of primary masses given earlier, and M_{tran} is the primary mass for transition from ECSN to ICCSN. For a Salpeter IMF, this ratio is 0.42 for $M_{tran} = 11M_{\odot}$ and 0.67 for $M_{tran} = 12M_{\odot}$. We take this ratio as 0.42 wherever it occurs in our calculations here.

4.3. Properties of the post-SN PDF

In order to appreciate the nature of the post-SN distribution, we calculate and plot the individual PDFs for each of these parameters, obtained by integrating \bar{f}_{psn} over the other two. We now discuss each of these distributions.

4.3.1. Companion mass

The distribution of the companion mass shows a slow early rise and then broken power-law behaviour with the break occurring at $\sim 30M_{\odot}$, as shown in Fig.1. The power-law slope is ≈ -2.4 , in the mass range $20 - 30M_{\odot}$, whereas above the break point the M_c -distribution becomes steeper, with a slope of ≈ -5.2 . The kink seen at the breakpoint of $30M_{\odot}$ becomes a *fold* in the bivariate distribution as a function of M_c and a (See Fig. 4). This kink appears at the mass which corresponds to the upper limit of the primary mass in the primordial binary. The allowed range of the primary mass is $9M_{\odot} \leq M_p \leq 30M_{\odot}$: this constraint was imposed to ensure the formation of neutron star as an end product of the stellar evolution of the primary.

It can be easily seen from the relation given above between the mass of the primary

and that of its He-core that the mass range obtained for M_c if we take $M_p = 30M_\odot$, corresponding to the entire allowed range of M_s , is $\approx 30M_\odot - 51M_\odot$. Thus for $M_c \leq 30M_\odot$, a large range of M_p can contribute, whereas for $M_c > 30M_\odot$ the allowed range of M_p is rapidly cut off as M_c increases, which causes a rapid reduction in the number of systems possible in this region. Thus, the effect of the allowed phase-space region is reflected in the transition in the power-law index of the M_c -distribution. In the region where large parts of the phase space of M_p are allowed to contribute, the slope of the PDF is close to the input IMF slope of -2.35 . For masses above the kink, only small parts can contribute, resulting in a steeper fall. For similar reasons of forbidden phase space, a downturn is expected at very low values of M_c , in the mass range $\sim (10 - 15)M_\odot$.

Upon inclusion of SN-kicks, the above mass distribution is essentially unchanged in the mid- M_c range, except that the kink at $\sim 30M_\odot$ becomes less prominent. But the distribution is cut off more sharply at the lowest and highest masses, the former being immediately understandable since kicks tend to preferentially unbind systems with lower binding energy.

The bivariate $M_c - a$ distribution shown in Fig.4 reveal the complexity introduced by the kicks. Although the surface shows similarities to its no-kick counterpart in general features, several additional features appear due to Maxwellian-averaged kicks corresponding to the two different values of σ given above for the two types of SN, namely, ECSN and ICCSN.

4.3.2. *Semimajor axis*

Fig.2 shows the PDF of $\log(a)$, the post-SN semimajor axis on a logarithmic scale. The PDF without considering the effect of SN-kicks is flat (*i.e.*, loguniform in a) in the mid- a

range, with smooth rise and fall at low and high values of a respectively. This is clearly a direct consequence of the assumed flat, Öpik’s-law distribution of primordial binaries, which remains unchanged at the intermediate values of a . The PDF with the SN-kicks included clearly shows two additional features. First, there is a general shift of the distribution towards wider orbits, entirely as expected, since SN-kicks generally tend to widen orbits. Second, the PDF is not exactly loguniform, *i.e.*, flat in the mid- a range now: a slow fall with increasing a is observed in this range, before the PDF falls off rapidly at large a , as before. This second feature is a consequence of the fact that SN-kicks steadily reduce the probability of survival of wider binaries even in the mid- a range, before destroying them altogether at large a -values.

4.3.3. Eccentricity

In the absence of kicks, the eccentricity introduced by the SN explosion is equal to the fractional mass loss from the system. As this fraction is small ($\sim 10\%$ or less) in case of HMXBs, only small eccentricities are introduced by the SN in the no-kick scenario. Figure 3, which shows the post-SN eccentricity PDF, confirms this. However, introduction of the SN-kicks changes this result completely, making the post-SN systems much more eccentric, as expected. Further, the results for ICCSN and ECSN are quite different in terms of post-SN eccentricity, also as expected because of the large difference between σ in the two cases (see above). Due to the small kicks imparted in case of ECSN with v_k^2 independent of the details of the pre-SN system (see Sec.3.2 and Appendix A), the eccentricities are generally smaller than in the ICCSN case (although larger than in the no-kick case), and the e-distribution is spread over a large range. By contrast, for ICCSN the kicks are much larger, leading to large eccentricities, as shown in Fig.3. Further, in this case v_k^2 is almost a fixed fraction of the disruption velocity of the pre-SN system for Maxwellian (and possibly

also for other similar) distributions, as explained in Appendix A, so that the e-distribution is narrowly peaked around a value determined by that fraction. It is likely that more detailed calculations would widen this peak somewhat, but no qualitative changes are expected. The composite PDF of eccentricity for ECSN and ICCSN naturally shows a double-peaked structure, as in Fig.3.

Of course, the e-distribution calculated above refers to the immediate post-SN systems, which are not observable as XRBs. These systems subsequently undergo tidal circularization rapidly, so that most of them become circular or nearly so by the time mass transfer begins and the system turns on as a HMXB. Since eccentricity is an irrelevant parameter at the HMXB stage, we integrate \bar{f}_{psn} over the eccentricity to obtain only the bivariate PDF as a function of M_c and a , which is shown in Fig.4.

5. Post-SN binary to HMXB

Post-SN systems evolve over the main-sequence lives of their companions as detached systems on a short timescale ($\sim 10^6$ years), during which the orbit is tidally circularized. Therefore, a bivariate post-SN PDF adequately describes the HMXB system, being given by:

$$f_{psn}(M_c, a) = \int_0^1 \bar{f}(M_c, a, e) de \quad (10)$$

Observed collective properties of HMXBs are usually given as distributions of their luminosities (L) (*i.e.*, the X-ray luminosity function or XLF) and orbital periods (P_b), instead of M_c and a , which we have worked with upto this point. In order to compare our results with observations, a further transformation $(M_c, a) \rightarrow (L, P_b)$ is therefore required now. P_b can be calculated for given values of M_c and a using Kepler's third law. If all the

masses and distances are expressed in the units of the solar values, then P_b in hours is given by:

$$P_b^2 = 7.72 \frac{a^3}{M_c + M_{NS}} \quad (11)$$

Here $M_{NS} = 1.4M_\odot$ is the mass of the neutron star. To calculate the luminosity as a function of M_c and a , prescriptions of the mass-loss rate from the companion and the capture mechanism by the neutron star are required.

The companion expands into a giant/supergiant after completing its main-sequence life, and loses mass by driving a strong stellar wind at a rate \dot{M}_w . The neutron star captures a fraction of this lost mass. The accretion rate onto the neutron star is then given by $\dot{M} = \dot{M}_w \times (\text{capture fraction})$. In this work, we assume that HMXBs are entirely *wind-fed giant/supergiant* systems, thus ignoring those systems in which a main-sequence companion close to its Roche lobe may drive a (weak) *atmospheric* Roche-lobe overflow. This is certainly justified at higher X-ray luminosities, since systems fed only by the latter mechanism would be found at the lowest end of the XLF. In a similar vein, we also do not include HMXBs with Be-star companions (see Sec.7.2), since the transient nature of these systems with low duty cycles implies a low *time-averaged* luminosity, which would put them, again, at the low end of a time-averaged XLF, which is generally difficult to determine.

The X-ray luminosity L is then given by the standard stellar-wind model, according to which the massive companion drives a wind mass-loss at a rate \dot{M}_w , and with a terminal wind speed of V_w . Of this, a fraction $\sim \left[\frac{GM_{NS}}{V_w^2 a} \right]^2$ (the capture fraction introduced above) is captured and accreted by the neutron star, and the gravitational energy release from this accretion generates the X-rays. In order to connect L to the stellar and orbital parameters, we first note that L is the rate of release of the gravitational energy of the accreted matter

and hence is directly proportional to accretion rate \dot{M} as

$$L = \frac{GM_{NS}\dot{M}}{R_{NS}}, \quad (12)$$

which we can express numerically as $L_{36} \approx 1.17\dot{M}_{-10}$, where L_{36} is L in units of 10^{36} ergs/s and \dot{M}_{-10} is \dot{M} in units of $10^{-10} M_{\odot}/\text{yr}$. Next, we note that the accretion rate \dot{M} is related to the wind mass-loss rate \dot{M}_w and the above capture fraction as

$$\dot{M} = \dot{M}_w \times \left[\frac{GM_{NS}}{V_w^2 a} \right]^2. \quad (13)$$

To proceed further, we need models of stellar winds, which we consider next.

5.1. Stellar wind models

Models of stellar wind relate the mass loss rate and the terminal velocity of the wind to stellar parameters like mass, radius and luminosity. In our case, these parameters are the mass of the companion, the radius of the companion R_c and the luminosity of the companion L_c . Some well-known stellar-wind models which we consider here are those due to Castor *et al.*, Kudritzki-Reimers, and Vink *et al.* (Castor et al. 1975; Reimers 1975; Kudritzki & Reimers 1978; Vink et al. 2000), which span the range from the classic CAK model (Castor et al. 1975) of the 1970s to the recent Vink *et al.* model (Vink et al. 2000).

The rates of mass loss in these models are given by:

$$\begin{aligned} \text{Kudritzki-Reimers : } \dot{M}_w &= \gamma_{\text{KR}} \frac{L_c R_c}{M_c} \\ \text{Castor } et al. : \dot{M}_w &= \gamma_{\text{CAK}} \frac{L_c R_c^{0.5}}{M_c^{0.5}} \\ \text{Vink } et al. \dot{M}_w &= \gamma_{\text{Vink}} \frac{L_c^{2.45} R_c^{-0.5}}{M_c^{1.3}} \end{aligned} \quad (14)$$

The constants γ_{KR} , γ_{CAK} , and γ_{Vink} are given in the original works. We use the KR model in our main work here, and summarize the effects of varying the stellar-wind model in Sec.6.4.1.

5.1.1. *Stellar models*

Results of numerical calculations of stellar evolution give stellar parameters like radius and luminosity as functions of the mass, metallicity and the age of the star. For using the above stellar-wind models in our calculations, we need these parameters for a given mass and metallicity of the wind-driving companion. In the spirit of our semi-analytic approach, we use the parameters given by Hurley, Pols and Tout (2000, henceforth HPT) in their comprehensive work on the construction of analytic approximations to the standard numerical results of stellar-evolutionary codes. The range of M_c shown in Fig.1 and discussed in Sec.4.3.1 leads to the conclusion that, except for a small region at the lower end of this range, the massive companions ignite He in the core while in the Hertzsprung gap (HG), while those in that small region do so at the top of the giant branch (GB). The companion's luminosity remains nearly constant in the HG, as discussed in HPT. Relevant fitting formulae for the luminosity and radius in the core Helium burning (CHeB) phase are given in Sec.5 of HPT, particularly Secs.5.1 and 5.3. We have used a metallicity $z = 0.02$ in our main calculations, varying it later to test its effect on HMXB distribution (see Sec.6.4.3).

The terminal velocity V_w which appears in Eqn.13 is of the order of escape velocity from the surface of the companion and hence can be taken as a function of M_c , so that the accretion rate can be expressed in the form:

$$\dot{M} \propto \frac{f(M_c)}{a^2}, \quad (15)$$

where the function $f(M_c) \sim \dot{M}_w/V_w^4$ contains the physics of wind mass-loss. Equation 15 gives the accretion rate as a function of M_c and a and so, along with Eqn.11, provides the transformation from (M_c, a) to (\dot{M}, P_b) ,

5.2. Transformation of parameters

Inverse transformations for eqns. 15 and 11 need to be obtained to transform the PDF. We first carry out the transformation from (M_c, a) to (\dot{M}, P_b) . We note here that the PDF as a function of \dot{M} and L will be identical up to a numerical factor since the two are linearly related to each other. The inverse transformation can become complicated because $f(M_c)$ can be a very complicated function and hence difficult to invert analytically. Our goal would, of course, be to construct a procedure that works with a general $f(M_c)$, so that the formalism can be applied to any model without changing the procedure. We first write the accretion rate as

$$\dot{M}_{-10} = 3.92 \frac{f(M_c)}{a^2}. \quad (16)$$

The numerical factor is so chosen that $\gamma_{\text{KR}} = 10^{-4}$; for other models the numerical constants can be appropriately adjusted in a similar way. With the aid of Eqns.11 and 13, we can eliminate a and write

$$g(M_c) = G(P_b, \dot{M}_{-10}), \quad (17)$$

where

$$\begin{aligned} g(M_c) &= \frac{f^3(M_c)}{(M_c + M_{NS})^2}. \\ G(P_b, \dot{M}_{-10}) &= 2.78 \times 10^{-4} \dot{M}_{-10}^3 P_b^4. \end{aligned} \quad (18)$$

This equation can be numerically solved to obtain M_c as a function of (P_b, \dot{M}_{-10}) , which is the first inverse transformation equation. After computing M_c numerically, a can be computed using

$$a = h(M_c)H(P_b, \dot{M}_{-10}), \quad (19)$$

where

$$\begin{aligned} h(M_c) &= \frac{M_c + M_{NS}}{f(M_c)}. \\ H(P_b, \dot{M}_{-10}) &= 3.3 \times 10^{-2} \dot{M}_{-10} P_b^2. \end{aligned} \quad (20)$$

Using these inverse transformations, we calculate the Jacobian. The partial derivatives take the following forms in terms of the functions $G(\dot{M}_{-10}, P_b)$, $H(\dot{M}_{-10}, P_b)$, $g(M_c)$ and $h(M_c)$:

$$\begin{aligned} \frac{\partial M_c}{\partial \dot{M}_{-10}} &= \frac{\partial G}{\partial \dot{M}_{-10}} \left(\frac{dg}{dM_c} \right)^{-1} \\ \frac{\partial M_c}{\partial P_b} &= \frac{\partial G}{\partial P_b} \left(\frac{dg}{dM_c} \right)^{-1} \\ \frac{\partial a}{\partial \dot{M}_{-10}} &= h \frac{\partial H}{\partial \dot{M}_{-10}} + H \frac{dh}{dM_c} \left(\frac{dg}{dM_c} \right)^{-1} \frac{\partial G}{\partial \dot{M}_{-10}} \\ \frac{\partial a}{\partial P_b} &= h \frac{\partial H}{\partial P_b} + H \frac{dh}{dM_c} \left(\frac{dg}{dM_c} \right)^{-1} \frac{\partial G}{\partial P_b} \end{aligned} \quad (21)$$

From eqs.(17), (19) & (21), we can calculate the Jacobian as a function of P_b and \dot{M}_{-10}

as:

$$J = \left[\frac{M_c + M_{NS}}{f(M_c)} \right]^3 \left\{ 3 \frac{df}{dM_c} - 2 \frac{f(M_c)}{M_c + M_{NS}} \right\}^{-1} \left[1.84 \times 10^{-5} \dot{M}_{-10}^3 P_b^5 \right] \quad (22)$$

5.3. Transformation of Distributions

The distribution of HMXBs in P_b and \dot{M}_{-10} can now be obtained with the aid of Eqs.(8) and (10). It is:

$$f_{HMXB}(P_b, \dot{M}_{-10}) = f_{PSN} \left(M_c(P_b, \dot{M}_{-10}), a(P_b, \dot{M}_{-10}) \right) \left| J(P_b, \dot{M}_{-10}) \right|, \quad (23)$$

and \dot{M} and L are of course proportional to each other, as explained above.

The resultant bivariate PDF $f_{HMXB}(L, P_b)$ is displayed as a surface in Fig.7, and the individual PDFs for the L - and P_b -distributions are shown in Figs.9 and 8 respectively. For obtaining the individual distribution of each variable, the bivariate distribution is integrated over the other variable, as explained earlier, the range of integration extending over only the allowed range of the concerned variable.

In Fig.6, we show the allowed region in the $L - P_b$ plane, which shows how the allowed region in the $M_c - a$ plane shown in Fig.5 is mapped onto the plane of the new variables. The effect of the above transformation is a rotation of the allowed zone in (P_b, L) plane. The simple bounds on parameters of primordial binaries given earlier transformed into a nearly rectangular allowed region in the parameter space (M_c, a) for post-SN binaries (see Fig.5). After transformation to the *HMXB parameters*, however, this allowed zone rotates into an inclined band, as shown in Fig.6. The boundaries given in this figure serve as integration limits for the calculation of the individual PDFs from the bivariate distribution in terms of L and P_b .

6. The HMXB Distribution

We now discuss the nature of the distributions of the luminosities and binary periods of HMXBs calculated above, and compare them with the current state of observational knowledge of these distributions. We emphasize that we are not attempting a detailed fit to the data at this stage, but focusing instead on a comparison between the general trends in calculated and observed distributions. The purpose of such a comparison is of course to determine if a more detailed computational scheme, *e.g.*, a numerical population synthesis, is worthwhile in the future for giving a more detailed account of the observations. A major virtue of an approach like ours is that it is capable, at least in principle, of assessing in a transparent way the relative importance of various components (*e.g.*, the role of the primordial binary distributions vis-a-vis that of the evolutionary processes like the first mass transfer and the SN) in determining the final HMXB distribution. Such an assessment helps greatly in planning the strategy of subsequent computational studies.

6.1. Orbital Period Distribution

The PDF of HMXBs as a function of P_b is obtained immediately by integrating f_{HMXB} given in Eqn.23 over the accretion rate. The computed P_b distribution without SN-kicks (see fig. 8) is rather similar to the corresponding post-SN a distribution, *i.e.*, a flat Öpik’s law in the mid-region ($P_b \sim 300 - 3 \times 10^4$ hrs), with a gradual rise to this flatness at shorter periods and a slightly sharper fall-off from it at longer periods. The distribution with the inclusion of SN-kicks also resembles the post-SN a distribution with SN-kicks: the rise now is more gradual, reaching a maximum at $P_b \sim 1000 - 1500$ hrs. Instead of a flat top, a slow fall is observed mid- P_b range, followed by a sharper fall-off at long periods, as before. The major and obvious difference between the two distributions is an overall shift towards wider orbits and longer periods when SN-kicks are included, entirely as expected

and as seen earlier in the post-SN a -distribution. We compare our theoretically obtained P_b -distribution with observations in Sec.6.3.

6.2. X-ray luminosity function

The XLF of HMXBs can be obtained by integrating Eqn.23 over P_b , using the limits described previously and carrying out a simple linear transformation for \dot{M}_{-10} to L_{36} . The XLF is given by:

$$f_L(L_{36}) = \frac{1}{1.17} \int f_{HMXB}(P_b, \dot{M}_{-10}) dP_b \quad (24)$$

where $\dot{M}_{-10} = L_{36}/1.17$. Figure 9 shows the numerically computed XLF. A broken power-law can be fitted to this computed XLF, with a cut-off at the neutron-star Eddington limit. Equation 25 gives the power-law exponents in the low and high luminosity regimes, obtained by least-squares fits to the computed XLF:

$$\frac{dN}{dL} \propto L^\eta \text{ with } \eta = \begin{cases} -1.63 & 0.65 < L_{36} < 7.5 \\ -0.98 & 10^{-3} < L_{36} < 10^{-2} \end{cases} \quad (25)$$

The XLF calculated without SN-kicks is also given for reference. It overlaps with the XLF with SN-kicks in the low-luminosity regime, and shows a slightly shallower power-law of exponent is $\eta = -1.43$ in the high-luminosity regime, the cross-over point being at $L_{cr} \approx 8 \times 10^{34}$ erg/s.

We now examine the effects of the various model parameters, *e.g.*, stellar-wind model, IMF slope, metallicity, and so on on our theoretical XLF.

6.3. Comparison with observations

6.3.1. The XLF

We first compare the calculated L -distribution of Fig. 9 with the observed distribution. The major feature of the observed L -distribution is a power law with a differential slope $dN/dL \propto L^{-1.6}$ over a wide range of luminosities $3 \times 10^{35} \text{erg/s} \leq L \leq 3 \times 10^{40} \text{erg/s}$. This is the so-called “universal” X-ray luminosity function (XLF) of HMXBs, obtained in the following way. Whereas the observed XLFs of various nearby early-type galaxies (*e.g.*, the Milky Way, SMC, M82 and M83, the Antennae, NGC 4736, and so on) follow this trend, their normalizations are not the same. However, when the XLF of a given galaxy is normalized by the current star-formation rate (SFR) in that galaxy, XLFs for all these galaxies fall essentially on top of each other, yielding the above “universal” XLF (Gilfanov 2004; Gilfanov et al. 2004a; Gilfanov et al. 2004b; Grimm et al. 2002; Grimm et al. 2003). This is due to the well-known fact that the strength of the HMXB population and their X-ray output is proportional to the current SFR, and is closely related to the discussion given in earlier on how the rapid HMXB evolution leads to a distribution of HMXBs which is, in effect, a “snapshot” of the galaxy taken at its current SFR.

In comparing calculated and observed XLFs, we note first that, since we confine ourselves to only neutron-star HMXBs in this work, our calculated XLF applies only to luminosities not exceeding the Eddington luminosity L_E for a $\sim 1.4M_\odot$ neutron star, *i.e.*, $\sim 2 \times 10^{38} \text{erg/s}$. The observed XLF extends upto almost 2 decades of luminosity above this, and the HMXBs at these higher luminosities are believed to be black-hole systems, with the possibility of both stellar-mass black holes and intermediate-mass black holes (at the highest luminosities) being present. We return to this question in more detail in Sec.7.3.

With this caveat in mind, we note that there is a remarkable agreement between the

calculated and observed XLFs in the luminosity range $3 \times 10^{35} \text{erg/s} \leq L \leq 10^{38} \text{erg/s}$, above which the calculated XLF cuts off at the Eddington limit for neutron stars, as expected, so that no comparison with observations is possible at higher L . Below $L \approx 3 \times 10^{35} \text{erg/s}$, there was no data when the works referred to at the beginning of this subsection were published. However, more recent *XMM – Newton* observations of the Magellanic Clouds have extended the XLF below this lower limit, down to about $L \approx 10^{34} \text{erg/s}$ or slightly lower, for SMC and LMC (Shtykovskiy & Gilfanov 2005a; Shtykovskiy & Gilfanov 2005b). The results indeed suggest a flattening of the XLF at low luminosities, and the best-fit differential slope of the observed XLF at these luminosities for SMC, which is given in the above reference as $-1.13_{-0.13}^{+0.3}$, is in fact almost consistent with our calculated slope at low luminosities, given in Fig.9 and Eq.(25). However, we must be cautious with our calculated XLF in the low-luminosity regime, since we have neglected (a) main-sequence companions undergoing atmospheric Roche-lobe overflow, and (b) Be-star companions in our calculations here, as explained above.

6.3.2. The P_b -distribution

Observations of HMXB orbital periods are available in substantial numbers only for our galaxy and the Magellanic Clouds. Measurements of orbital periods have been performed for ~ 80 systems (Liu et al. 2005; Liu et al. 2006). Figure10 shows the distribution of orbital periods constructed with this data. The distribution shows a rising part in the range $10 - 300$ hrs. With the (large) error bars, the distribution in the region $P_b \approx 300 - 10000$ hrs is consistent with either a uniform trend or a slow rise/decay with a peak around $P_b \approx 2000$ hrs. It can be seen that our theoretical P_b -distribution is generally consistent with the observed one within the error bars, except at very long orbital periods, where the observed distribution shows a sharp cut-off beyond orbital periods ~ 1 year. Such an apparent cut-off

is expected for two observational reasons. First, it is very difficult to follow systems with such long orbital periods for sufficient times to establish reliable orbital periods. Second, such wide binary systems would generally have low luminosities, which would put them at the faint end of the XLF, and add further to the difficulties of a successful observation. Thus strong selection effects work against observation of HMXBs with long orbital periods. By contrast, the theoretical distribution extends upto the widest orbits that can survive the basic processes involved, particularly the SN explosion. The fact that these very wide binaries do not show up in the observed distribution does not imply that they do not exist, but simply that they are unobservable in practice.

6.4. Parameter Study

We now examine the effects of the various model parameters, *e.g.*, stellar-wind model, IMF, metallicity, and so on on our theoretical XLF.

6.4.1. Effects of stellar wind models

We consider the two alternative models by CAK and Vink *et al.*, which were introduced in Sec.5.1. XLFs computed for these models are shown in Fig.11. It can be seen that the XLFs overlap in the low-luminosity regime for all models, which means that the XLF is independent of the exact form of $f(M_c)$ (see above) in this region. The XLF's differential slope is close to -1 in this regime. The position of the cross-over luminosity L_{cr} is different for the three models with similar power-law exponents above respective L_{cr} . The CAK model cuts off rather abruptly at luminosities considerably below the Eddington luminosity of neutron stars and so appears unable to account for the observations. Barring the difference in the L_{cr} , the Kudritzki-Reimers model and the Vink model give similar results,

in general agreement with observations.

6.4.2. *Effects of the IMF slope*

The IMF is typically given as a single power-law in the mass range that is relevant to the problem at hand. The power-law index of the IMF (α) is considered to be within the range $\sim 2.0 - 2.7$, $\alpha = 2.35$ being the standard value given by Salpeter and widely used in this mass range. We study the effect of varying α on XLF in the range 2.0 - 3.0. The effect is shown in the Fig.11. The XLF at low luminosities below the kink shows hardly any variation. We therefore display the XLF only for luminosities above the kink. Even above the kink, the XLF slope varies by a small amount (from -1.47 to -1.66 between the lower and upper limits to α considered here), showing relative insensitivity of the XLF to the IMF slope. For an exact matching with the observed XLF, a slightly steeper IMF seems to be preferred, if other parameters remain unchanged.

6.4.3. *Other effects*

Among other parameters in the problem, we consider the stellar-wind velocity V_w and the metallicity z . The terminal velocity of the wind is an important factor in determining the capture fraction. It is typically of the order of the escape velocity at the surface of the companion and generally thought to be $\sim 10^3$ km/s. We varied V_w around this canonical value to test the effect on the XLF. The changes in both the XLF slope and the high-luminosity cutoff were insignificant.

Consider next the metallicity z , which affects the stellar parameters and the wind mass loss rate. We considered a large range of z from 10^{-4} to 0.02, and used the model of Vink *et al.* (2001) to study the effects of varying z on our final results. The results are shown

in Fig.12. There is no significant difference between the XLFs for $z = 0.01$ and $z = 0.02$: both have a slope ≈ -1.6 in the luminosity range $2 \times 10^{37} - 2 \times 10^{38} \text{ erg s}^{-1}$. The XLF for $z = 0.001$ also has nearly the same slope, but a somewhat different crossover luminosity. Finally, the XLF for $z = 10^{-4}$ is markedly different, but such low metallicities are not realistic for HMXBs, as they would be expected only in old stellar systems.

7. Discussion

In this work, we have developed a straightforward, first-principles scheme for understanding collective properties of HMXB populations, starting from standard, well-known collective properties of primordial binaries which are the progenitors of HMXBs, and following the transformations of the probability distributions through the evolutionary processes that lead to the formation of HMXBs. Our purpose, of course, was to assess if the standard picture of primordial binaries and the standard evolutionary scenario for HMXBs together can account for the observed collective properties of HMXBs in a basic, simple way. The fact that we find that such an account can indeed be given is most encouraging, and it constitutes, in our view, an essential step towards attempts at elaborate population synthesis schemes designed for understanding further details of these collective properties. Since our procedure is transparent and readily understandable at each step, it is easy in our scheme to follow the role of each ingredient in shaping the final HMXB distribution. In this section, we discuss various issues of principle and procedure which are relevant to this line of approach, and conclude with plans for the future.

7.1. Primordial-binary mass distribution

We pointed out in Sec.2.1 that distributions of the masses M_p, M_s of the primary and secondary in the primordial binary can be described either in terms of these masses themselves, *i.e.*, the pair (M_p, M_s) , or alternatively in terms of the primary mass and the mass ratio $q \equiv M_s/M_p$, *i.e.*, the pair (M_p, q) . Both have been done in the literature (Warner 1961; Jaschek & Ferrer 1972; Halbwachs 1983; Trimble 1990; Kouwenhoven et al. 2007; Kobulnicky & Fryer 2007), and we have chosen here the second description for its closer correspondence with essentially all recent work. The relation between these two approaches has been discussed thoroughly by Tout (1991).

7.2. Be-star binaries

Massive companions in HMXBs are of two types in general, *viz.*, OB giants/supergiants and Be stars, the latter being characterized by (a) strong, broad emission lines that supply evidence for rapid stellar rotation, and (b) somewhat lower masses and wider orbits. Since we have confined our detailed calculations in this work to the former, as stated in Sec.5, we now discuss the expected role of Be-star binaries in HMXB XLF.

It is believed that Be stars are often surrounded by an outflowing disk of matter expelled by centrifugal forces from the fast-roating equatorial regions of the star, in addition to the usual stellar wind emitted from all over the stellar surface. Accretion by the neutron star from this outflow material generally follows the basic description from stellar winds given in Sec.5.1, with appropriate values of V_w for the fast wind and the slowly outflowing disk, with one major caveat. Since the matter in the rapidly-rotating outflow disk has much angular momentum, it may form an *accretion* disk around the neutron star, which would then drain on the neutron star a slow, viscous timescale. This complicates the description

considerably, as the outflow disk is generally expected to be tilted with respect to the orbital plane (Ghosh 1995), so that the orbiting neutron star would “crash” through this outflow disk (twice per orbit in general), possibly acquire an accretion disk, and accrete it slowly over the rest of the orbit. This would naturally lead to outbursts of X-ray emission, which are indeed observed in Be-star HMXBs.

The question for our purposes here is: how does all this affect the XLF of HMXBs? First consider the observational situation. The point to note here is that Be-star HMXBs are basically transient systems with low duty cycles, so that a long-term average of the luminosity of a Be-system is much lower than that of an OB supergiant-system. Thus, in an XLF constructed from a long-term monitoring of the X-ray sky with an all-sky monitor, one would expect the high- L parts to be dominated by OB-systems, while the low- L parts may have considerable contributions from Be-systems. Indeed, the observed XLFs cited earlier in this paper have been constructed from recent work with X-ray observatories in the following way. The XLF for the Milky Way has been constructed from ~ 4 years of observation with the all-sky monitor on *RXTE*. Thus, the above argument certainly applies to this case. Indeed, since the typical long-term average expected from Be-systems would be at or below the lower end of the luminosity-range over which the XLF is actually reported (and this applies to basically all observed XLFs except those obtained from *XMM – Newton* observations of SMC and LMC; see Sec.6.3.1), we would expect little contribution to the reported XLF from Be-star systems.

However, note that the XLF for other nearby galaxies reported in these references have been constructed essentially from one “snapshot” (*i.e.*, a single exposure) taken by *Chandra* and *XMM – Newton* (Gilfanov 2004). Given this, it is remarkable that the XLFs of all these galaxies (suitably normalized by their SFRs) are essentially coincident with one another over the same range of L , as explained earlier. Considering the fact that,

because of their low duty cycles, only a small fraction of the Be-systems would be present in these “snapshot” XLFs, we would still expect some contribution from them in a range of L typical of the outbursts of Be-systems. The fact that these XLFs appear very similar to the above long-term average XLF of the Milky Way over the canonical luminosity range $3 \times 10^{35} \text{ergs}^{-1} \leq L \leq 3 \times 10^{40} \text{ergs}^{-1}$ is therefore most noteworthy, and may imply that, for reasons which are not clear at present, Be-systems may not have made a substantial contribution to these observed XLFs.

Now consider the inclusion of Be-systems in calculational schemes like ours. To the extent that the wind-accretion formalism can be applied to accretion from both the fast, low-density wind from the stellar surface and the slow, high-density outflow in the equatorial disk (Ghosh 1995), these systems are already in our scheme, at least in principle. However, while a quantitative description of the periodic acquisition and drainage of accretion disks described above has been done for individual binary systems (Pravdo & Ghosh 2001), its inclusion in a study of collective properties of HMXB populations is more complex and outside the scope of this work.

7.3. Black-hole HMXBs and ULXs

As mentioned in Sec.6.3.1, the observed “universal” XLF of HMXBs extends to about two decades of luminosity above the Eddington luminosity for canonical $1.4M_{\odot}$ neutron stars. While we focus on neutron-star HMXBs in this study, it is interesting to consider this brightest end of the XLF briefly. If the X-ray sources here are accretion-powered, they can only contain accreting black holes (some sources upto luminosities $\sim 10^{39} \text{erg s}^{-1}$ can of course be close juxtapositions of several neutron-star sources, as has sometimes been suggested), either stellar-mass ones ($M_{BH} \sim 10M_{\odot}$), or even the so-called intermediate-mass black holes (IMBH), with masses $M_{BH} \sim (10^2 - 10^5)M_{\odot}$, the X-ray sources corresponding

to the latter objects being often called ultra-luminous X-ray sources (ULX).

A truly remarkable feature of the universal HMXB XLF is that a single, smooth power law gives an excellent account of X-ray binaries containing neutron stars, stellar-mass black holes, and IMBHs over the entire luminosity range $3 \times 10^{35} \text{ergs}^{-1} \leq L \leq 3 \times 10^{40} \text{ergs}^{-1}$, *i.e.*, above the “kink” in the XLF (Gilfanov 2004). While it is not difficult to extend the formation and evolution scenario outlined in the earlier sections to include higher primary masses which would produce stellar-mass black holes, and then imagine that the other systematics would go through in such a way as to extend the power-law XLF, this argument does not automatically include ULXs and IMBHs, whose formation scenario has to be different and more exotic, *e.g.*, black-hole mergers in dense stellar clusters. And yet, as Gilfanov (2004) has noted, these “rare” and “exotic” objects appear to form a smooth extension of the “ordinary” HMXB population. Whether this is really true or not can possibly be probed with future observations in a way suggested by this author: if we adopt the alternative hypothesis that the apparent cutoff in the currently observed XLF at $L \sim 3 \times 10^{40} \text{ergs}^{-1}$ really corresponds to the maximum possible luminosity of what we may call “ordinary”, stellar-mass black holes referred to above, then these “exotic” IMBHs may show up beyond this cutoff if we can observe regions with extremely high star-formation rates, since the merger scenario for the formation of IMBHs implies that they would occur in very dense regions with very high star-formation rates. However, since such IMBHs would necessarily be rarer than stellar-mass black holes, we should expect a “step down” at the presently observed cutoff, beyond which the XLF would continue at a lower strength. This is a fascinating possibility.

7.4. Shape of the XLF

Understanding the XLF shape is an important step towards extracting information about various processes which determine the collective properties of HMXBs. Two main features of the XLF calculated using our scheme are (1) A kink at $L_{cr} \approx 8 \times 10^{34}$ erg/s, and (2) a power-law behavior with the differential slope of -1.6 above L_{cr} . We will discuss the possible origin of these two features in this section.

7.4.1. The XLF kink

The origin of the kink in the HMXB XLF can be understood in terms of allowed zones in the parameter space. This is demonstrated in a clear way by overplotting contours of constant L on the allowed zone in the (M_c, a) plane, as shown in Fig.5. Let us first examine a simple “toy” model for the XLF. In this model, we approximate the post-SN PDF as a function of M_c and a as $f_{psn} \propto M_c^{-\alpha}/a$ (as discussed earlier, this “toy” is not too bad an approximation over much of the parameter range in case of no SN-kicks). We now note that L can be written in a schematic way as $L \propto f(M_c)/a^2$. Next we transform the approximate form of the post-SN PDF from (M_c, a) to (M_c, L) . A bit of simple algebra shows that such a transformation gives a PDF of the form $f_H \propto M_c^{-\alpha}/L$. Integrating this PDF over M_c would yield $dN/dL \propto L^{-1}$, if the limits of integration were independent of L . Figure 5 shows that this is indeed the case for $10^{33} \text{erg/s} \leq L \leq L_{cr}$, since the M_c -limits are clearly seen to be almost independent of L when L lies in this range.

By contrast, as we move to higher L -values, the contours become shorter by cutting off low- M_c regions. In other words, the lower limit of integration becomes a function of L . Shortening of the contour length results in a power-law XLF with the slope steeper than -1. Eventually, near the neutron-star Eddington luminosity, the contour passes out of the

allowed region altogether, and the XLF is cut off.

At very low luminosities we expect a similar mechanism to cause a turnover in the XLF (which would cut it off eventually at extremely low luminosities), as is clear from Fig.5, since higher- M_c regions are progressively cut off as L decreases in this range. However, this effect is not expected to be very important for two reasons. First, cutting of the highest-mass regime in M_c is not a severe problem, since the M_c -distribution drops steeply in that regime anyway. Therefore, one needs to go to very low luminosities ($\leq 10^{32}$ erg/s) to observe this effect. Second, with current observational sensitivity, we can track the XLF behavior below L_{cr} only for a few nearby galaxies, and the very low luminosities indicated above are not even approached. It appears, therefore, that this XLF turnover is unlikely to be amenable to observation in the near future, and accordingly we do not consider it any further.

7.4.2. *The XLF slope*

The XLF of HMXBs obtained observationally does not reach luminosities below L_{cr} for most of the galaxies (see Sec.6.3). Therefore, only the power-law regime above L_{cr} can be compared with observations in most cases. Physical origins of this power-law index are an important aspect of our understanding of the collective properties of HMXBs. Note first that our calculation of the XLF is a numerical one, and the power-law result given in Sec. 6.2 is only an analytic approximation to it. However, simple qualitative arguments may serve to illustrate the basic physics underlying such calculations, and we consider such arguments below.

In a pioneering argument of this type, Postnov (2003; also see Postnov & Kuranov 2005) proceeded as follows. Expressing the XLF as:

$$\frac{dN}{dL} = \frac{dN}{dM_c} \frac{dM_c}{dL}, \quad (26)$$

one can use a suitable estimate of the mass-function dN/dM_c of the companion for these arguments. The estimation of $\frac{dM_c}{dL}$ is more involved, and the original Postnov method was to estimate $\frac{dL}{dM_c}$ as follows, and use its reciprocal. Using $L \propto \dot{M} \propto \dot{M}_w/(a^2 V_w^4)$ (see Sec.5), this author obtained a power-law form $L \propto M_c^\beta$, with the aid of a simple stellar-wind model $\dot{M}_w \propto L_c/V_w \propto L_c \sqrt{R_c/M_c}$, into which the following scalings for massive stars were inserted: $L_c \propto M_c^3$, $R_c \propto M_c^{0.8}$. This gave $\beta \approx 2.5$. Finally, assuming a power-law form for the companion mass distribution, *i.e.*, $dN/dM_c \propto M_c^{-\alpha}$, straightforward algebra with Eq.(26) leads to an XLF slope of $dN/dL \propto L^{-(\alpha+\beta-1)/\beta}$. Postnov (2003) assumed $\alpha = 2.35$ (*i.e.*, the exponent of the Salpeter IMF) for the M_c -distribution, which led to an XLF slope of ≈ -1.54 .

In revisiting the above argument, we note first that Eq.(26) is incomplete, since N is a function of both M_c and a , whose form we have calculated explicitly in the earlier sections. Thus, the complete equation is

$$\frac{dN}{dL} = \frac{\partial N}{\partial M_c} \frac{dM_c}{dL} + \frac{\partial N}{\partial a} \frac{da}{dL}. \quad (27)$$

Next, we note that the scalings of L_c and R_c with M_c used in the Postnov (2003) work apply to massive *main-sequence* stars, but not to the evolved massive stars of interest here. Also, the wind mass-loss prescription used in that work is similar to that in the CAK model of the 1970s, which our calculations have shown to be inadequate. The rough scalings for L_c and R_c for evolved massive companions of interest here can be obtained from the appropriate formulae in Sec.5 of HPT, and are $L_c \propto M_c^{1.8}$, $R_c \propto M_c^{4.6}$.

With these scalings, and our M_c -distribution shown in Fig.1, which we can approximate

with the power-law of exponent $\alpha = 2.4$ that applies to its principal part, we can evaluate the first term on the right-hand side of Eq.(27). For the Kudritzki-Reimers model, it can be easily shown that $\beta \approx 5.4$, so that this first term gives an XLF slope $-(\alpha + \beta - 1)/\beta \approx -1.27$. The other stellar model gives an essentially identical final result. The rest of the contribution comes from the second term on the right-hand side of Eq.(27), which can be easily calculated and which leads to our overall XLF slope ≈ -1.63 .

We have gone through this argument in detail because it addresses an interesting observation made by Gilfanov (2004) that, in HMXB systems powered by stellar-wind accretion, the distribution of \dot{M} and therefore L should be governed by the properties of the massive companion, in particular the distribution of M_c and L_c . Our work here shows that this is largely, but not completely, true. The properties of the massive companion are contained in the first term on the right-hand side of Eq.(27), and keeping only this term, as Postnov (2003) did, amounts to neglecting altogether the binary orbital properties which are contained in the second term on the right-hand side of Eq.(27), and which also influence the XLF. The estimates summarized above give a measure of the relative sizes of the effects of the companion and the orbit, and demonstrate that, while the latter are certainly smaller, they are by no means negligible.

7.5. Conclusions and outlook

In this work, we have described a method for obtaining the distributions of some of the essential collective properties of HMXB populations in the stellar fields of normal/starburst galaxies, wherein we start from accepted distributions of primordial binaries which are progenitors of such HMXBs, and follow the transformation of these distributions with the aid of a Jacobian formalism as the primordial binary population evolves into the HMXB population. Our method, which is semi-analytic, traces in a transparent way the effects of

various processes in the course of this evolution, and so assesses with ease which physical processes dominate in determining which distribution. For example, the distribution of the properties of the massive companions seems to have the dominant effect on the XLF, although the distribution of the orbital parameters does have a significant effect, as we demonstrated in Sec.7.4.2. But the distribution of HMXB orbital periods appears to be strongly influenced by both the primordial orbital distribution and the SN-kick properties.

The agreement between our calculated XLF and binary-period distribution and the observed HMXB distributions is most encouraging, and it justifies a future Monte Carlo population synthesis scheme for a more detailed understanding of how HMXB populations are built in the stellar fields of normal galaxies. However, we must first extend our present method to the more complex problem of following the formation and evolution of LMXB populations from their corresponding primordial binaries, as mentioned in Sec.1. This will occupy us in the next papers in this series.

It is a pleasure to thank M. Gilfanov, E. P. J. van den Heuvel, V. Kalogera, L. Stella, and R. A. Sunyaev for stimulating discussions, and an anonymous referee for valuable comments which greatly improved the paper.

A. Averaging supernova kicks and post-SN transformation equations

A.1. Calculation of SN-kick average

In this appendix we describe the method of averaging the effects of SN-kicks for a Maxwellian kick-distribution. It has been widely assumed that the distribution of kicks will be isotropic and recent observations by have supported it (Hobbs et al. 2003). Therefore the angle dependence in Eq.5 is averaged in a straightforward way, which leads to Eq.6.

Two points are to be noted here. First, the only surviving kick-term in the averaged transformation equations is v_k^2 which is to be obtained by averaging v^2 over the Maxwellian distribution. Second, it must be remembered that the process of averaging gives the average values of post-SN quantities. These therefore should be compared with the average behaviour of a number of sample observational sets.

A further, most crucial, point to be noted at this stage is that in our study here (and in all similar studies), we are interested in *only* those post-SN systems which remain bound as XRBs, so that they can eventually produce HMXBs whose distribution we are interested in. Accordingly, we must exclude at this point all systems which become unbound in the SN. The way we do so is as follows. We note that, in the v^2 -averaging process, we would make an error if we carried out the integrations over the Maxwellians in Eq.7 upto infinitely large values of v , since this would include all the unbound systems that are to be excluded. Rather, we must *truncate* the integration at a suitable upper limit v_{up} which corresponds to the point at which the post-SN system becomes just unbound. This point is readily obtained from the first of Eqns.6 by setting $a_f \rightarrow \infty$, and v_{up} given by:

$$v_{up} = \sqrt{\frac{M_i^t}{a_i} \left(1 - \frac{2\Delta M}{M_i^t} \right)} \quad (\text{A1})$$

We thus work with a Maxwellian which is truncated from above at v_{up} (and suitably normalised), so that v_k^2 is given by:

$$v_k^2 = \frac{\int_0^{v_{up}} v^4 \exp(-v^2/2\sigma^2) dv}{\int_0^{v_{up}} v^2 \exp(-v^2/2\sigma^2) dv} \quad (\text{A2})$$

v_{up} is well-defined for each set of values of pre-SN parameters. For algebraic convenience, we can express it as $v_{up} = f\sqrt{2}\sigma$ for a given Maxwellian distribution with dispersion σ . This simplifies the expression for v_k^2 , which can be written as $v_k^2 = \sigma^2 h(f)$,

where $h(f)$ is given by:

$$\begin{aligned} h(f) &= 3 - \frac{2f^2 h_2(f)}{h_1(f) - h_2(f)} \\ h_1(f) &= \sqrt{\frac{\pi}{2}} \text{Erf}(f) \\ h_2(f) &= f\sqrt{2}e^{-f^2} \end{aligned} \tag{A3}$$

Fig.13 shows $h(f)$ as a function of f . Two regimes are clearly demarcated, with a small transition region between the two. The low- f region can be described by a power-law given by, $h(f) = 1.2f^2$, whereas in the high- f region, $h(f) = 3$, which is its asymptotic value. The crossover point of the two regimes is at $f_c \approx \sqrt{2.5}$. This clear division in two regions give us a straightforward relation for v_k^2 . For $f < f_c$, v_k^2 is independent of σ , and is given by $v_k^2 = 0.6v_{up}^2$. On the other hand, for $f > f_c$ v_k^2 is independent of v_{up} , and is given by $v_k^2 = 3\sigma^2$. This behavior of $h(f)$ can be understood as follows. For $f < f_c$, v_{up} is small and hence only the initial rising part of the Maxwellian is relevant. Thus the distribution is essentially given by $f(v) \propto v^2$, which is independent of σ . On the contrary, for $f > f_c$, v_{up} is large and almost the entire Maxwellian profile is included, excluding only a small tail. Detailed calculations given above show that the transition region between these two regimes is small, so that, as a first approximation, we can use the following simple prescription:

$$v_k^2 = \begin{cases} 0.6v_{up}^2 & f < f_c \\ 3\sigma^2 & f > f_c \end{cases} \quad \text{where } f_c = \sqrt{2.5} \tag{A4}$$

The above prescription can be substituted appropriately in eqn. 6 to obtain the post-SN parameter transformation or the inverse transformation, which is required for the Jacobian formalism. We describe in the next section the relevant transformation equations and the Jacobian for the two cases.

A.2. Post-SN parameter transformation

For $f > f_c$

In this region, v_k^2 is independent of the parameters of the binary system. We can simplify Eqn.6 by using following ratios. Let $r_i = M_i^t/a_i$, $r_f = M_f^t/a_f$, and $r_k = \sigma^2$. Also, we define orbit size change factor as $s = a_f/a_i$. Equation 6 can then be used to write the inverse transformations:

$$\begin{aligned} s &= \frac{1 + \sqrt{e^2(1 + r_k/r_f) - r_k/r_f}}{1 - e^2} \\ r_i &= r_f(2s - 1) - 3r_k \end{aligned} \tag{A5}$$

These equations are indirect transformations which give a_i and M_i^t on substituting the definitions of s and r_i in above equations. Since the companion mass is unchanged in the SN explosion, one can readily calculate $M_{p,c}$ from M_i^t for known M_c . The Jacobian of this transformation can be calculated as follows. Note first that the transformation is only in two variables *i.e.* $(a_f, e) \rightarrow (a_i, M_{p,c})$, since the third parameter *i.e.* M_c is unchanged. For the same reason, one can also write $\partial M_{p,c}/\partial(a, e) = \partial M_i^t/\partial(a, e)$. All the necessary partial derivatives can be written in terms of the derivatives of s and r_i as follows:

$$\begin{aligned} \frac{\partial a_i}{\partial a_f} &= \frac{1}{s} - \frac{a_f}{s^2} \frac{\partial s}{\partial a_f} \\ \frac{\partial a_i}{\partial e} &= \frac{a_f}{s^2} \frac{\partial s}{\partial e} \\ \frac{\partial M_i^t}{\partial(a_f, e)} &= a_i \frac{\partial r_i}{\partial(a_f, e)} + r_i \frac{\partial a_i}{\partial(a_f, e)} \\ J_{sn} &= \left| \frac{\partial M_{p,c}}{\partial e} \frac{\partial a_i}{\partial a_f} - \frac{\partial M_{p,c}}{\partial a_f} \frac{\partial a_i}{\partial e} \right| \end{aligned} \tag{A6}$$

For $f < f_c$

v_k^2 in this region is independent of σ and written only in terms of v_{up} , which is given by eqn. A1. The inverse transformations in this case are given by:

$$\begin{aligned} s &= \frac{1 + \sqrt{(3e^2 - 1)/2}}{1 - e^2} \\ M_i^t &= \frac{M_f^t}{3} [5s(1 - e^2) - 4] \end{aligned} \quad (\text{A7})$$

where s is the orbital-size factor defined similarly as a_f/a_i . The Jacobian in this case is given by an even simpler relation. One can easily see that M_i^t is independent of a_f and depends only on e . Therefore $\partial M_i^t / \partial a_f = 0$. The Jacobian in that case is given by $J_{sn} = (\partial M_i^t / \partial e)(\partial a_i / \partial a_f)$. Straightforward algebra shows that

$$J_{sn} = \frac{5}{2s} \frac{M_f^t e}{s(1 - e^2) + 1} \quad (\text{A8})$$

These two inverse transformations can be applied in the relevant regions to transform the PDF with the aid of the Jacobian formalism.

REFERENCES

- Arzoumanian, Z., Chernov, D. F., and Cordes, J. M. 2002, ApJ, 568, 289
- Belczynski, K., Kalogera, V., Rasio, F. A., Taam, R. E., Zezas, A., Bulik, T., Maccarone, T. J., and Ivanova, N. 2008, ApJS, 174, 223
- Banerjee, S., and Ghosh, P. 2006, MNRAS, 373, 1188
- Banerjee, S., and Ghosh, P. 2007, ApJ, 670, 1090
- Banerjee, S., and Ghosh, P. 2008, ApJ, 680, 1438
- Castor, J. I., Abbott, D. C., and Klein, R. I. 1975, ApJ, 195, 157.
- Davidson, K. and Ostriker, J. P. 1973, ApJ, 179, 585.
- Ghosh, P. 1995, ApJ, 453, 411
- Ghosh, P. 2007, *Rotation and Accretion Powered Pulsars*, World Scientific, Singapore.
- Ghosh, P., and White, N. 2001, ApJ, 559, L97
- Giacconi, R., Gursky, H., Kellogg, E., Schreier, E. & Tananbaum, H. 1971, ApJ, 167, L67.
- Gilfanov, M. 2004, Prog Theo Phys Suppl, 155, 49.
- Gilfanov, M. , Grimm, H.-J., and Sunyaev, R. 2004a, Nucl Phys B Proc Suppl, 132, 369.
- Gilfanov, M. , Grimm, H.-J., and Sunyaev, R. 2004b, MNRAS, 347, L57.
- H.-J. Grimm, Gilfanov, M. , and Sunyaev 2002, A&A, 391, 923.
- H.-J. Grimm, Gilfanov, M. , and Sunyaev 2003 ChJAS, 3 (supplement), 257.
- Halbwachs, J. L. 1983, A&A, 128, 399.

- Heger, A., et al., 2003. *ApJ*, 591, 288
- Hobbs, G., Lorimer, D. R., Lyne, A. G., and Kramer, M. 2005, *MNRAS*, 360, 974
- Hurley, J., Pols, O., and Tout, C. 2000, *MNRAS*, 315, 543
- Jaschek, C., and Ferrer, O. 1972, *PASP*, 84, 292.
- Kalogera, V. 1996, *ApJ*, 471, 352
- Kim, D.-W., and Fabbiano, G., *ApJ*, 611, 846
- Kim, D.-W., and Fabbiano, G., *ApJ*, 721, 1523
- Kobulnicky, H., and Fryer, C. 2007, *ApJ*, 670, 747
- Kouwenhoven, M., et al. 2007, *A&A*, 474, 77
- Kroupa, P. and Weidner, C. 2003, *ApJ*, 598, 1076
- Kudritzki, R., and Reimers, D. 1978, *A&A*, 70, 227.
- Lamb, F. K., Pethick, C. J. and Pines, D. 1973, *ApJ*, 184, 271.
- Linden, T., Sepinsky, J. F., Kalogera, V., and Belczynski, K. 2009, *ApJ*, 699, 1573
- Liu, Q. Z., van Paradijs, J. and van den Heuvel, E. P.J. 2005, *A&A*, 442, 1135.
- Liu, Q. Z., van Paradijs, J. and van den Heuvel, E. P.J. 2006, *A&A*, 455, 1165
- Madau, P., Pozzetti, L., and Dickinson, M. 1998, *MNRAS*, 498, 106
- Öpik, E. 1924, *Tartu Obs Publ*, 25, No. 6.
- Podsiadlowski, P., Langer, N., Poelarends, A. J. T., Rappaport, S., Heger, A., and Pfahl,
E. 2004, *ApJ*, 612, 1044

- Postnov, K. 2003, *Astr Let*, 29, 372
- Postnov, K., and Kuranov A. 2005, *Astr Let*, 31, 7
- Pravdo, S., and Ghosh, P. 2001, *ApJ*, 554, 383
- Pringle, J. E. and Rees, M. J. 1972, *A&A*, 21, 1.
- Reimers, D. 1975, *Mem Soc Roy Sci Liège*, 6e serie, 8, 369.
- Salpeter, E. E. 1955, *ApJ*, 121, 161
- Sana, H., and Evans, C. 2011, in *Active OB stars*, Proc IAU Symp 272, eds. C. Neiner et al., in press.
- Scheck, L., Kifonidis, K., Janka, H.-T., and Müller, E. 2006, *A&A*, 457, 963
- Scheck, L., Plewa, T., Janka, H.-T., Kifonidis, K., and Müller, E. 2004, *Phys. Rev. Lett.*, 92, 011103
- Shapiro, S. L. and Teukolsky, S. A. 1983, *Black Holes, White Dwarfs, and Neutron Stars: The Physics of Compact Objects*, Wiley & Sons, New York.
- Shtykovskiy, P. and Gilfanov, M. 2005a, *MNRAS*, 362, 879.
- Shtykovskiy, P. and Gilfanov, M. 2005b, *A&A*, 431, 597.
- Tout, C. 1991, *MNRAS*, 250, 701.
- Trimble, V. 1990, *MNRAS*, 242, 79.
- van den Heuvel, E. P. J. 1983, in *Accretion-driven stellar X-ray sources*, eds. W. H. G. Lewin and E. P. J. van den Heuvel, Cambridge Univ. Press, Cambridge, p. 303.

- van den Heuvel, E. P. J. 1991, in *Neutron stars: theory and observation*, eds. J. Ventura and D. Pines, Kluwer, Dordrecht, p. 171.
- van den Heuvel, E. P. J. 1992, in *X-ray binaries and recycled pulsars*, eds. E. P. J. van den Heuvel and S. A. Rappaport, Kluwer, Dordrecht, p. 233.
- van den Heuvel, E. P. J. 2001, in *The neutron star-black hole connection*, eds. C. Kouveliotou et al., Kluwer, Dordrecht, p. 173.
- Vink, J. S., de Koter, A., and Lamers, H. J. G. L. M. 2000, A&A, 362, 295.
- Vink, J. S., de Koter, A., and Lamers, H. J. G. L. M. 2001, A&A, 369, 574.
- Warner, B. 1961, PASP, 73, 439.

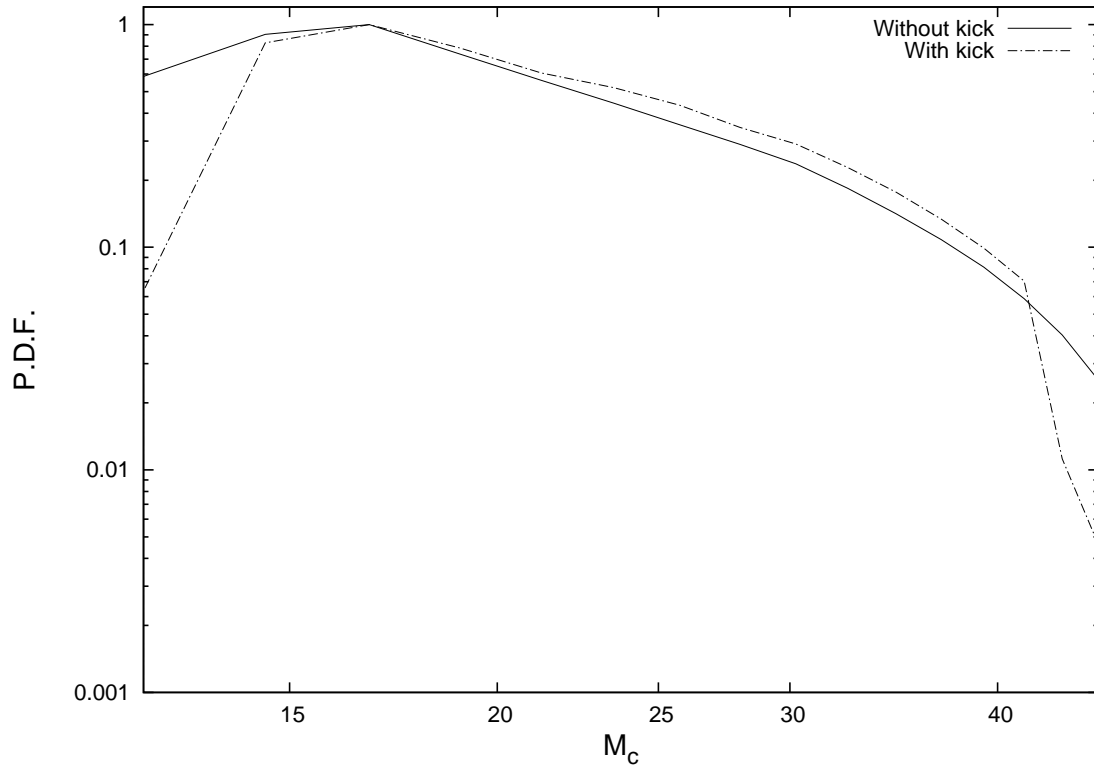


Fig. 1.— Distribution of companion masses in post-SN systems.

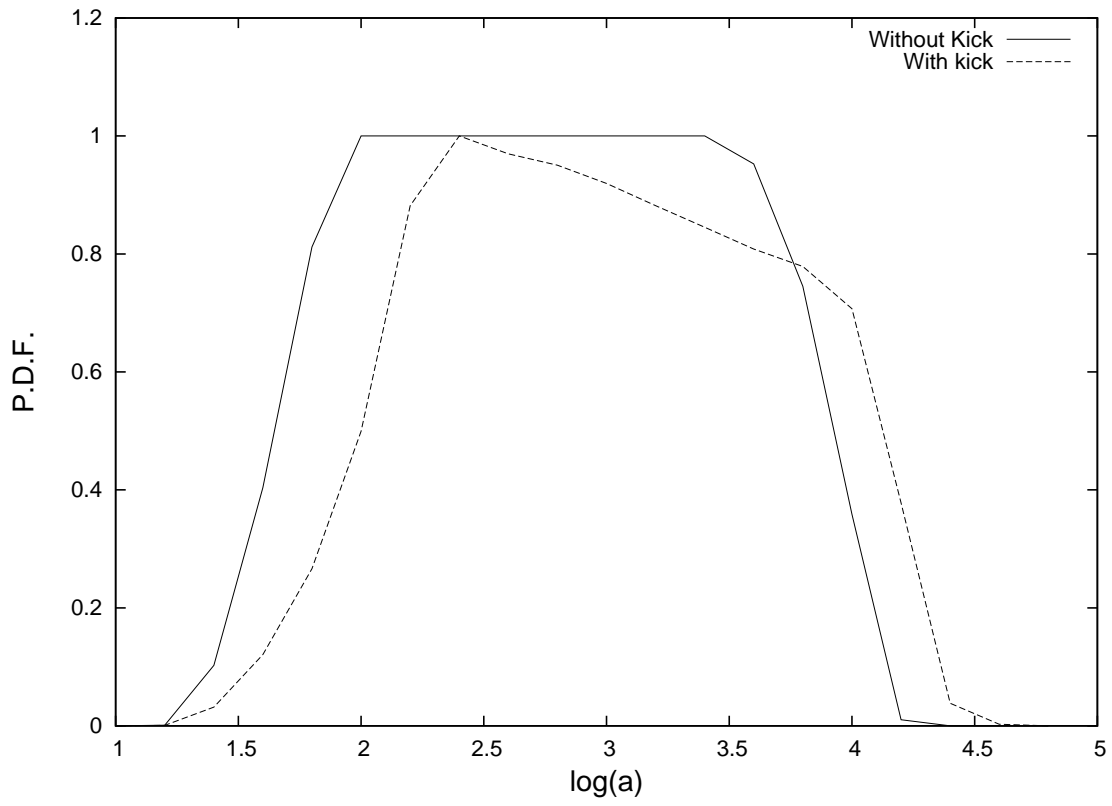


Fig. 2.— Distribution of semi-major axes of post-SN systems.

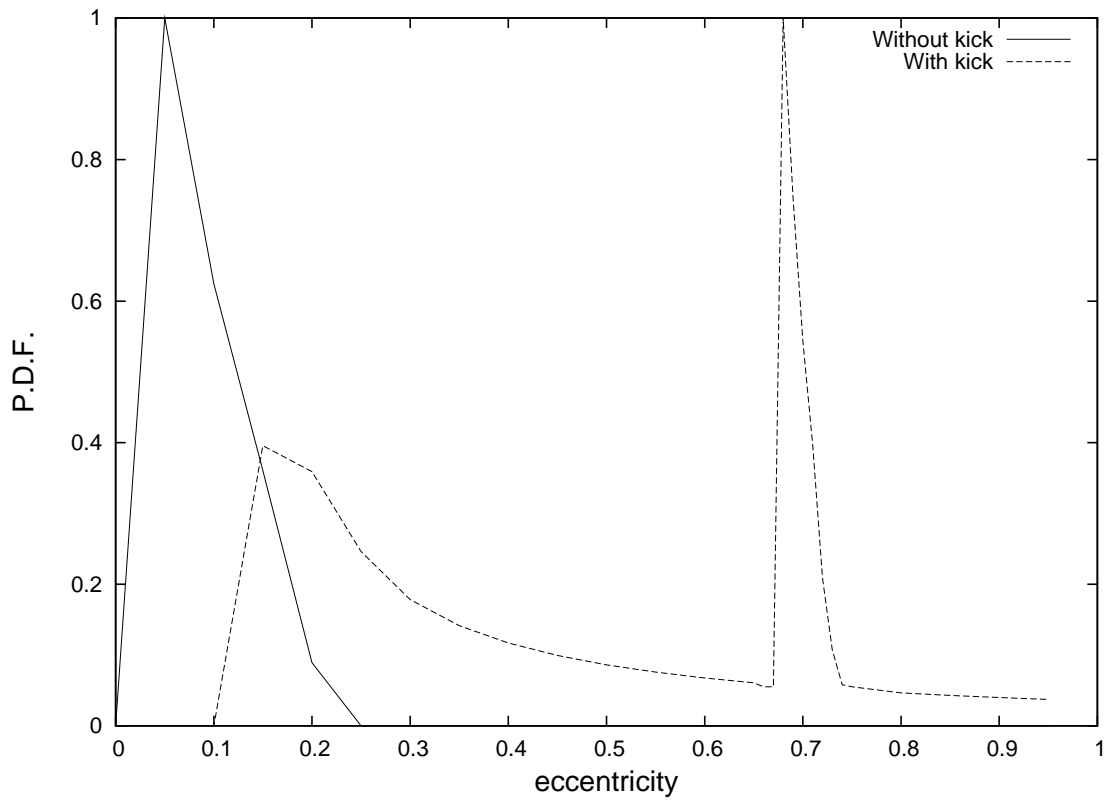


Fig. 3.— Distribution of eccentricities of post-SN systems.

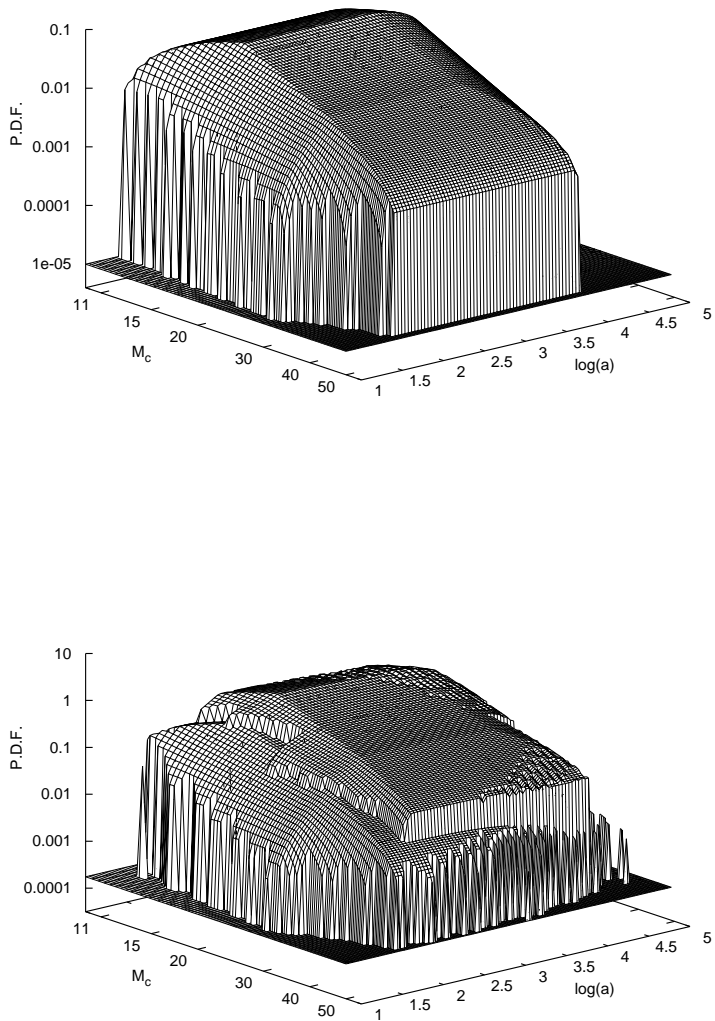


Fig. 4.— Bivariate distribution of post-SN systems as a function of both M_c and a . Left panel: Without SN-kicks. Right panel: With SN-kicks included.

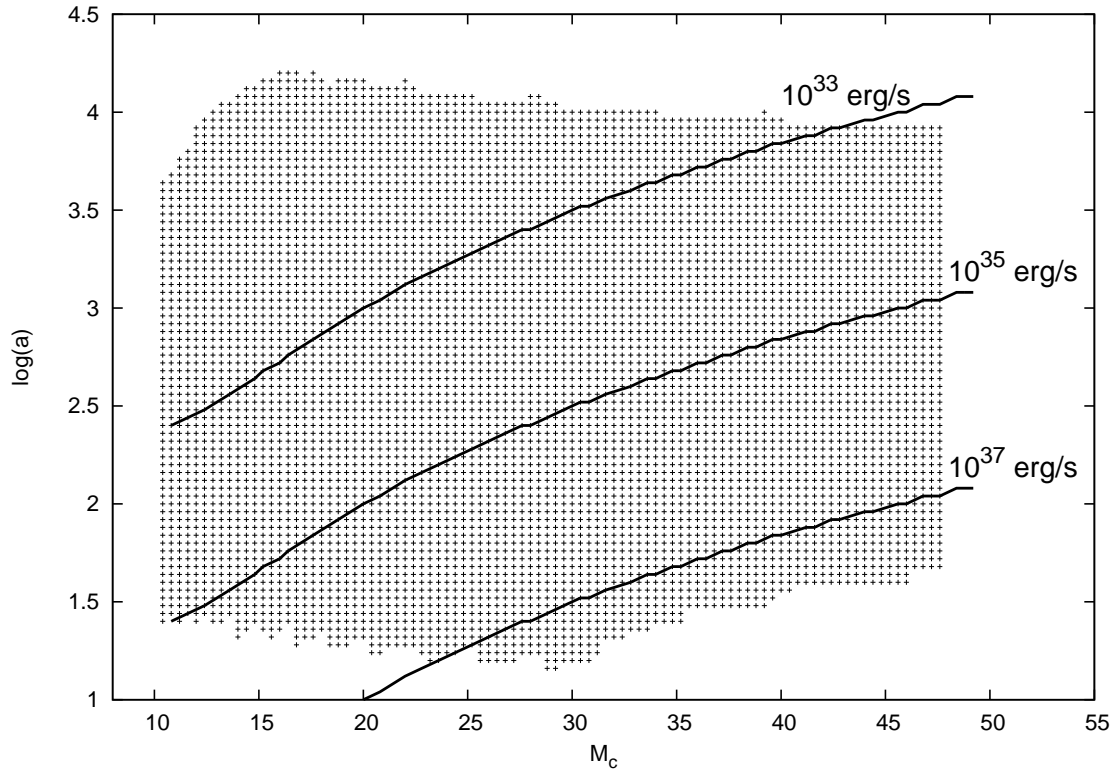


Fig. 5.— Allowed zone in $M_c - a$ parameter space, shown as shaded area. Overplotted are contours of constant L , each contour labeled by its value of L .

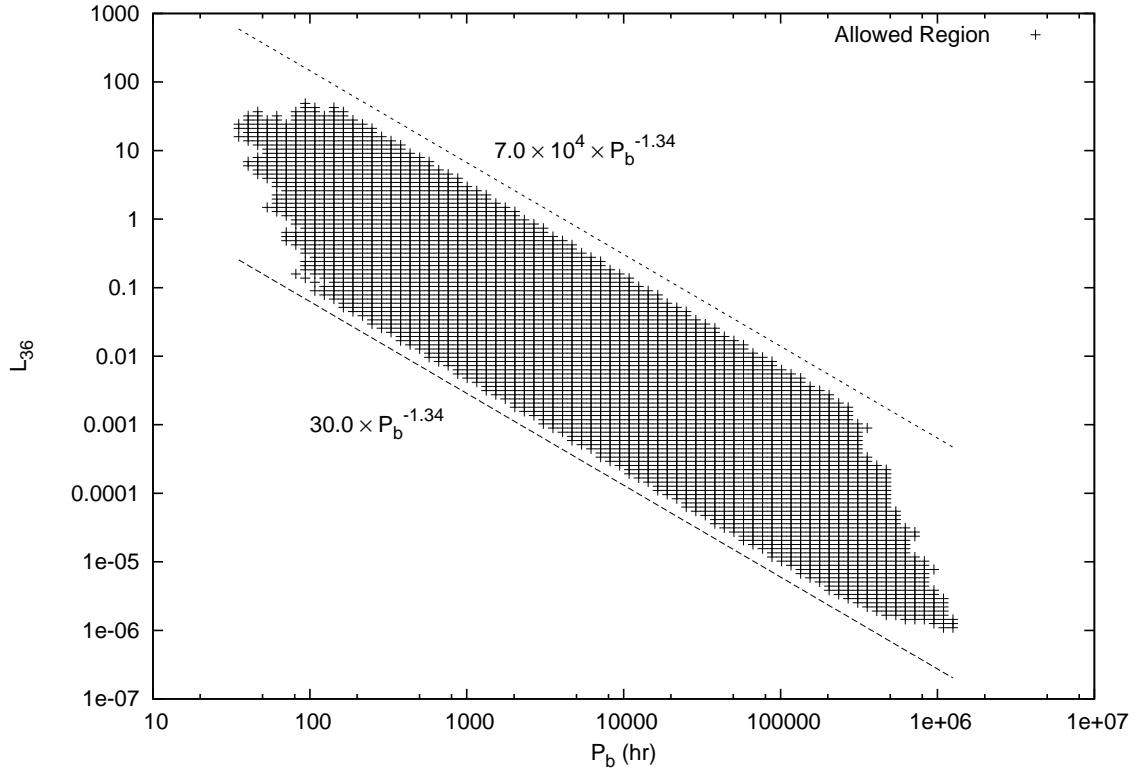


Fig. 6.— Allowed zone in $L-P_b$ space shown covered by crosses. Upper and lower boundaries of zone as indicated.

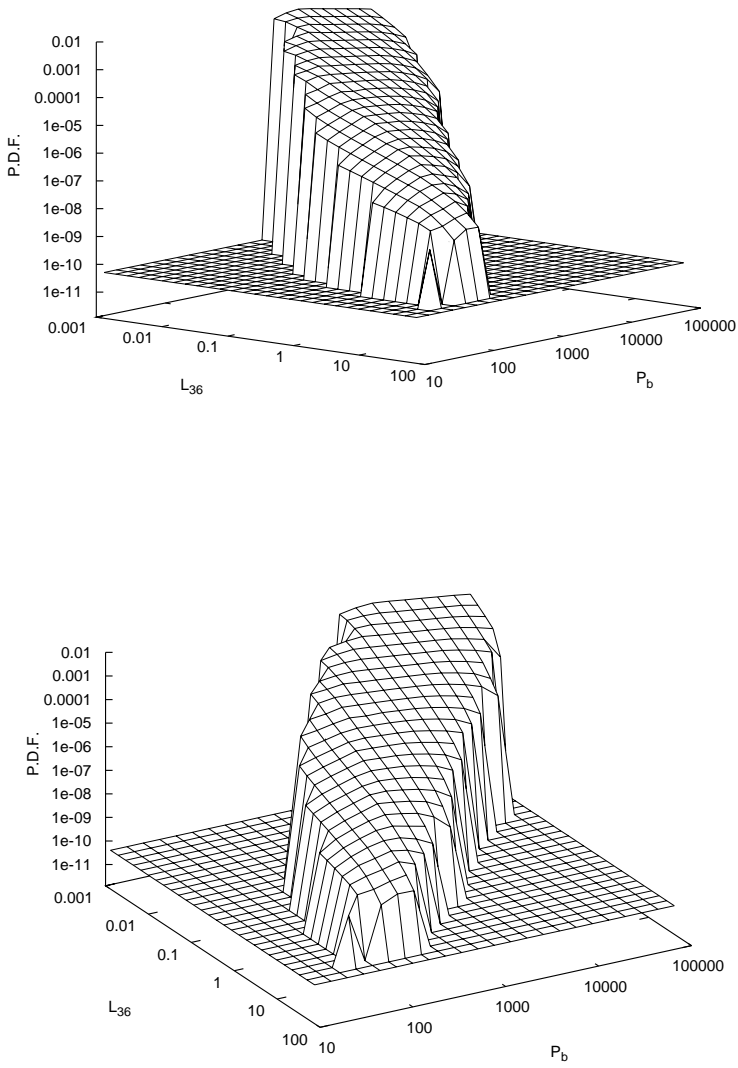


Fig. 7.— Bivariate distribution of HMXBs as a function of both L and P_b , including the effects of SN-kicks. Two views of the 3-dimensional figure are shown in order to bring out the trends with L (left panel) and P_b (right panel).

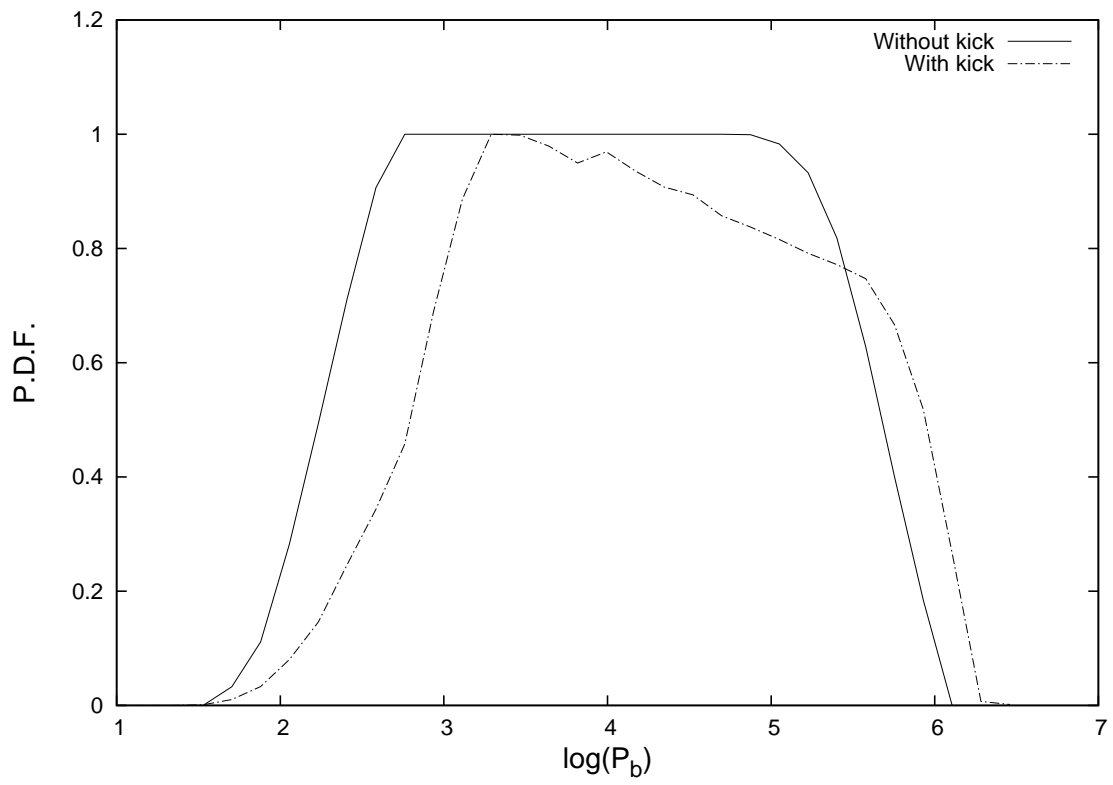


Fig. 8.— Calculated distribution of HMXB orbital periods.

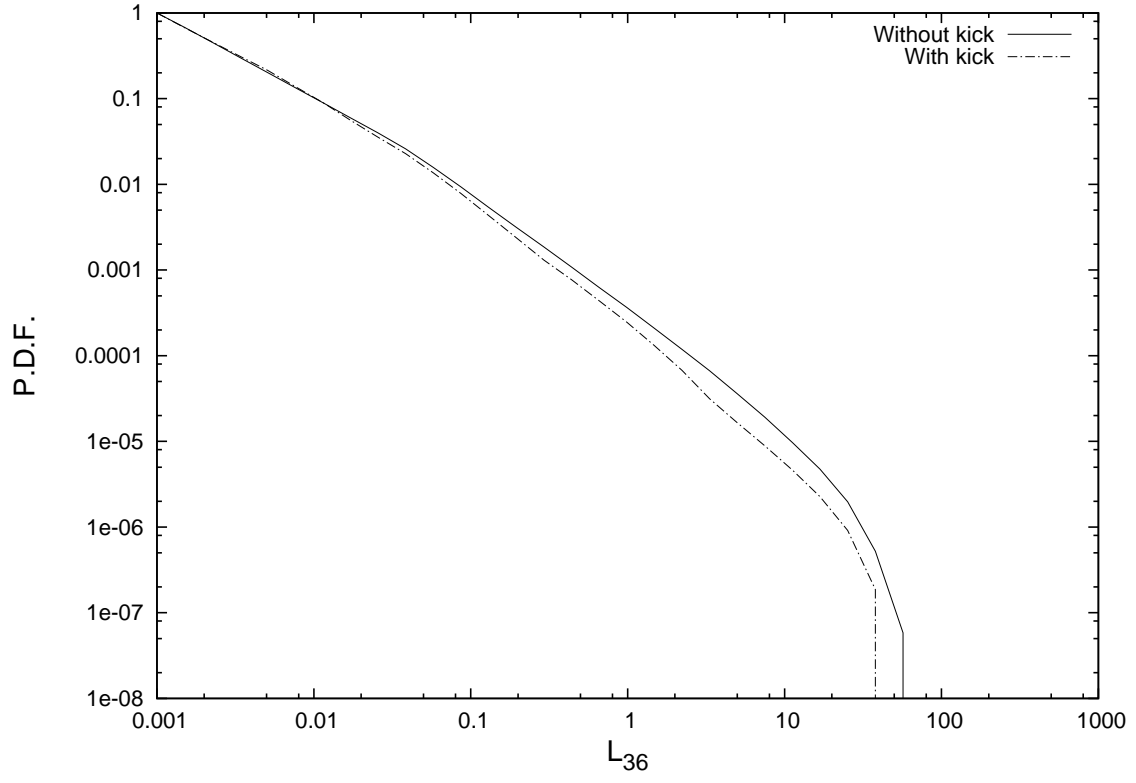


Fig. 9.— Calculated XLF of HMXBs.

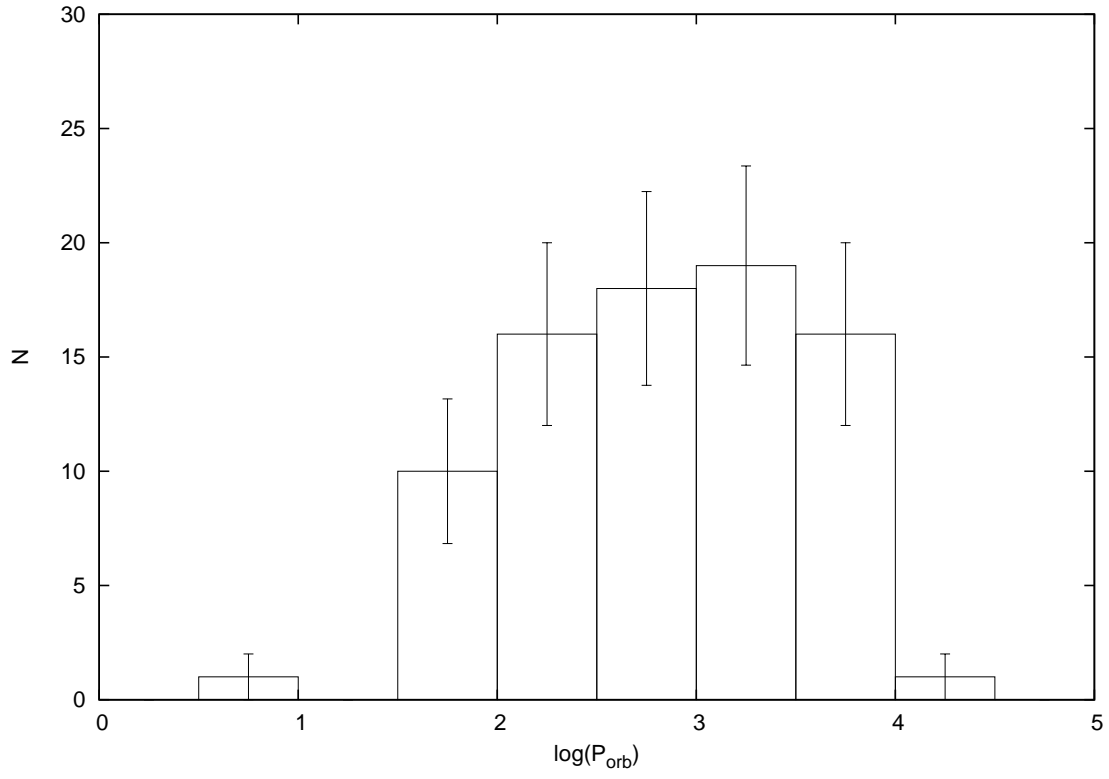


Fig. 10.— Observed distribution of HMXB orbital periods. Shown is the data for ~ 80 systems in the Milky way, SMC and LMC. From the catalogues by Liu *et al.*: see text.

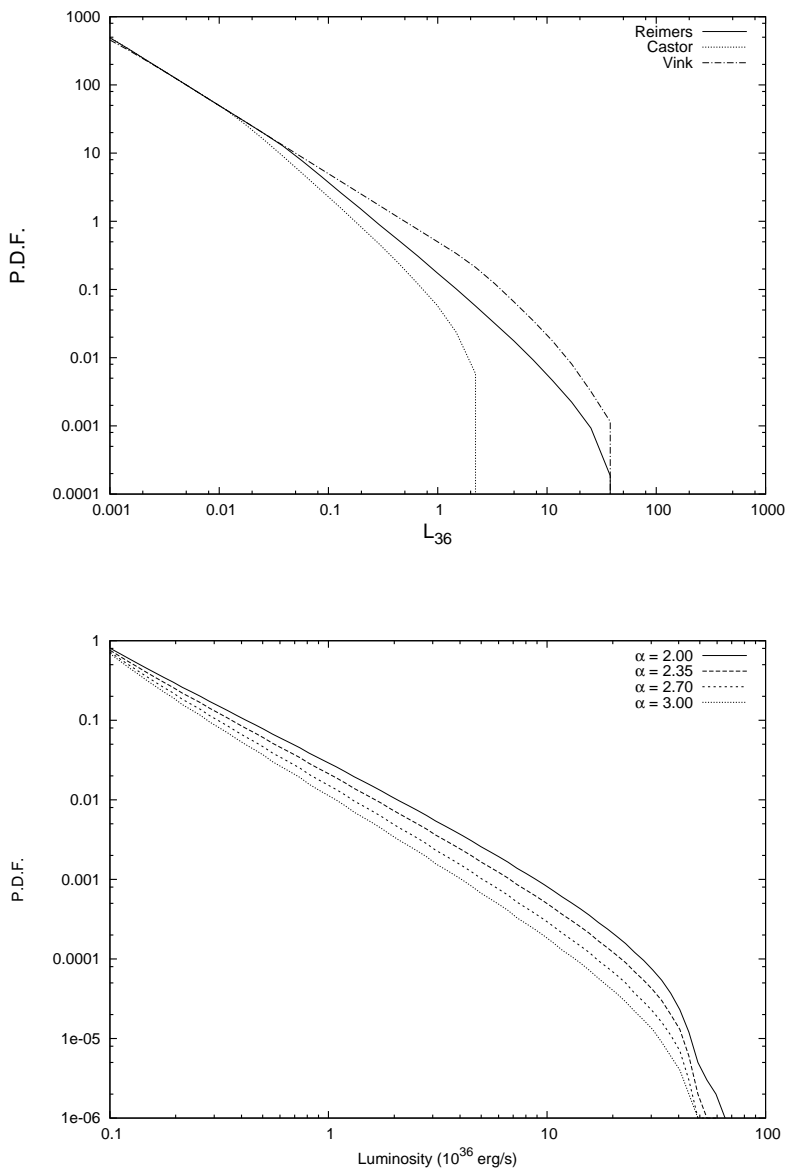


Fig. 11.— Dependence of XLF on model parameters. Left panel: different stellar wind models, as labeled. Right panel: different IMF slopes, as labeled.

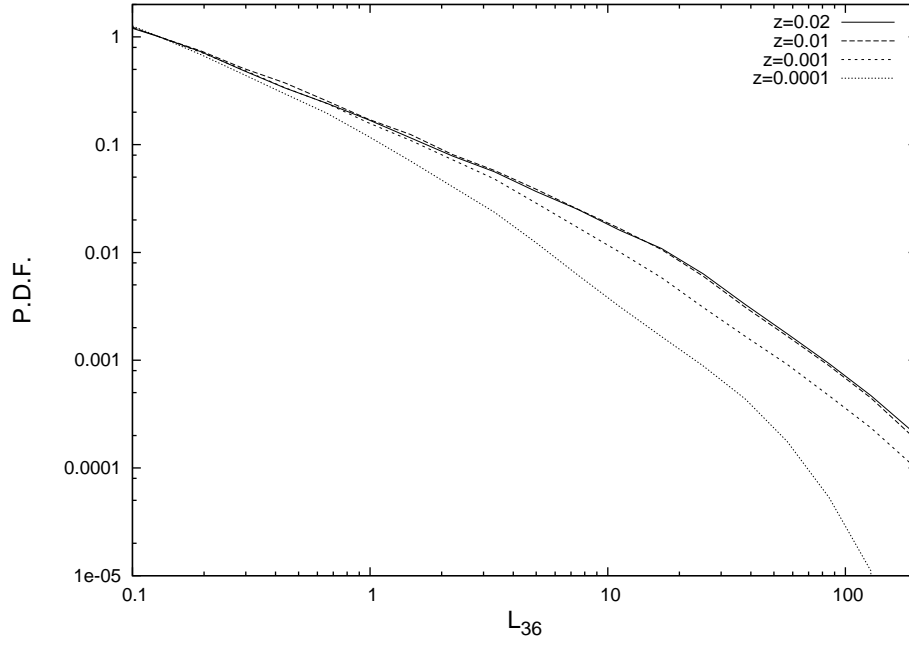


Fig. 12.— Dependence of XLF on model parameters: metallicity z , as labeled.

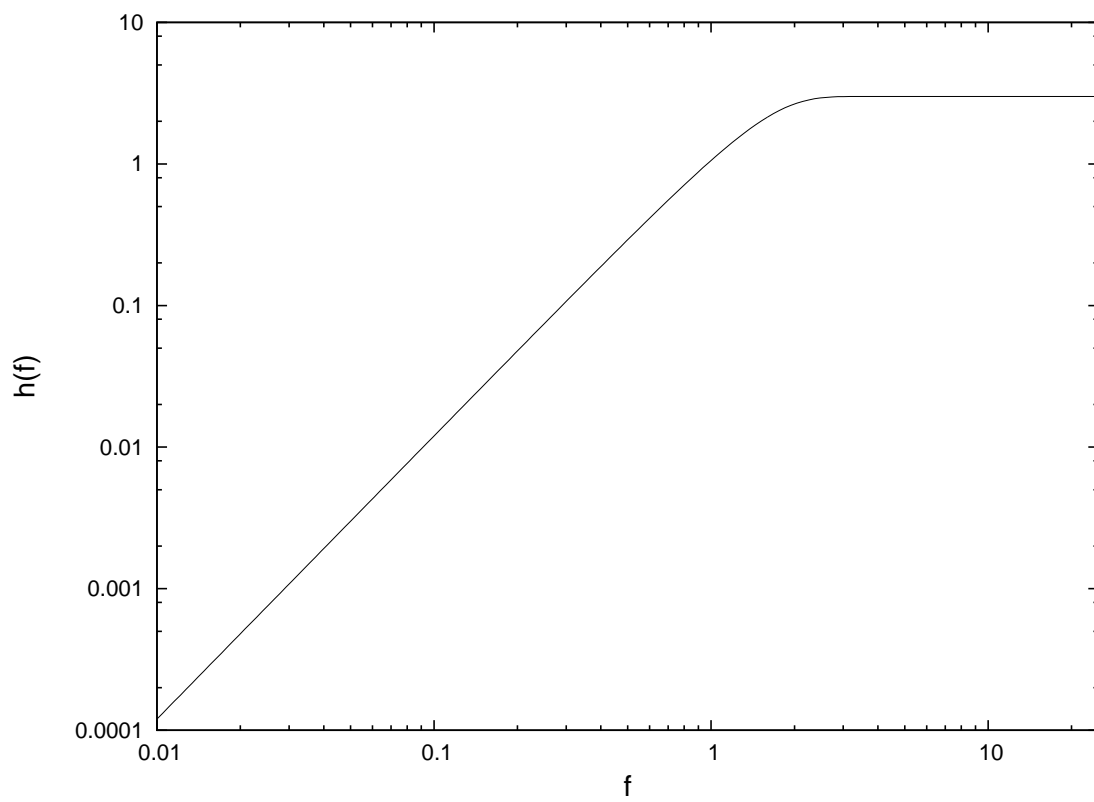


Fig. 13.— Dependence of $h(f)$ on f